

Article

Characterization of a Metamorphosed Volcanic Stratigraphy and VMS Alteration Halos Using Rock Chip Petrography and Litho geochemistry: A Case Study from King North, Yilgarn Craton, Western Australia

Jamie Kelly ¹, Steven P. Hollis ^{2,*}, Cendi D. P. Dana ², Allan Kneeshaw ³, Darryl Podmore ³, Megan James ³, Riquan Azri ³, Conal Rodgers ² and Stephen Roberts ¹

¹ School of Ocean and Earth Science, National Oceanography Centre, University of Southampton, Southampton SO14 3ZH, UK; jamie.kelly@soton.ac.uk (J.K.); sr2@soton.ac.uk (S.R.)

² School of GeoSciences, Grant Institute, The University of Edinburgh, James Hutton Road, King's Buildings, Edinburgh EH9 3FE, UK; c.d.p.dana@sms.ed.ac.uk (C.D.P.D.); conalrodgers1@googlemail.com (C.R.)

³ Black Raven Mining, 282 Welshpool Road, Welshpool 6106, Australia; adkneeshaw@gmail.com (A.K.); darryl.podmore@blackravenmining.com.au (D.P.); megron1@bigpond.com (M.J.); riquanazri@gmail.com (R.A.)

* Correspondence: steven.hollis@ed.ac.uk

Abstract: Despite countless advances in recent years, exploration for volcanogenic massive sulfide (VMS) deposits remains challenging. This is particularly the case in the Yilgarn Craton of Western Australia, where outcrop is limited, weathering is deep and extensive, and metamorphism is variable. At Erayinia in the southern Kurnalpi terrane, intercepts of VMS-style mineralization occur along ~35 km strike length of stratigraphy, and a small Zn (-Cu) deposit has been defined at King (2.15 Mt at 3.47% Zn). An extensive aircore and reverse circulation drilling campaign on the regional stratigraphy identified additional VMS targets, including the King North prospect. Through a combination of detailed rock chip logging, petrography (inc. SEM imaging), and litho geochemistry, we have reconstructed the volcanic stratigraphy and alteration halos associated with the King North prospect. Hydrothermal alteration assemblages and geochemical characteristics at King North (Mg-Si-K enrichment, Na depletion, and high Sb, Tl, Eu/Eu*, alteration index, CCPI, and normative corundum abundance values) are consistent with an overturned VMS system. The overturned footwall stratigraphy at King North is dominated by metamorphosed volcanic rocks, namely the following: garnet amphibolite (tholeiitic, basaltic), biotite amphibolite (andesitic, calc-alkaline), chlorite-quartz schist (dacitic), and narrow horizons of muscovite-quartz schist (dacitic to rhyolitic, HFSE-enriched). The hanging-wall to the Zn-bearing sequence is characterized by quartz-albite schists (metasedimentary rocks) and thick sequences of amphibolite (calc-alkaline, basaltic andesite). An iron-rich unit (>25% Fe₂O₃) of chlorite-actinolite-quartz schist, interpreted as a meta-exhalite, is associated with significant Cu-Au mineralization, adjacent to a likely syn-volcanic fault. Extensive Mg metasomatism of the immediate felsic footwall is represented by muscovite-chlorite schist. Diamond drilling into the deep hanging-wall stratigraphy at both King North and King has also revealed the potential for additional, stacked VMS prospective horizons in the greenstone belt stratigraphy. The discovery of HFSE-enriched rhyolites, zones of muscovite-chlorite schist, presence of abundant sulfide-rich argillaceous metasedimentary rocks, and a second upper meta-exhalite horizon further expand the exploration potential of the King-King North region. Our combined petrographic and litho geochemical approach demonstrates that complex volcanic lithologies and VMS alteration signatures can be established across variably metamorphosed greenstone belts. This has wider implications for more cost-effective exploration across the Yilgarn Craton, utilizing RC drilling to reconstruct the local geology and identify proximal halos, and limiting more costly diamond drilling to key areas of complex geology and deeper EM targets.

Keywords: volcanic-hosted massive sulfide; VHMS; exploration; Yilgarn Craton



Citation: Kelly, J.; Hollis, S.P.; Dana, C.D.P.; Kneeshaw, A.; Podmore, D.; James, M.; Azri, R.; Rodgers, C.; Roberts, S. Characterization of a Metamorphosed Volcanic Stratigraphy and VMS Alteration Halos Using Rock Chip Petrography and Litho geochemistry: A Case Study from King North, Yilgarn Craton, Western Australia. *Minerals* **2024**, *14*, 481. <https://doi.org/10.3390/min14050481>

Academic Editors: Stavros Triantafyllidis and Stylianos Tombros

Received: 25 March 2024

Revised: 29 April 2024

Accepted: 29 April 2024

Published: 30 April 2024



Copyright: © 2024 by the authors. Licensee MDPI, Basel, Switzerland. This article is an open access article distributed under the terms and conditions of the Creative Commons Attribution (CC BY) license (<https://creativecommons.org/licenses/by/4.0/>).

1. Introduction

Despite countless advances in recent years, exploration for volcanogenic massive sulfide (VMS) deposits remains challenging. This is particularly the case in the Yilgarn Craton of Western Australia, where outcrop is limited, weathering is deep and extensive, and metamorphism is variable [1,2]. VMS exploration in the Yilgarn Craton (Figure 1), like that in other Archean cratons worldwide, focuses on greenstone belts where submarine volcanic activity was coeval with both crustal extension and the emplacement of large, shallow subvolcanic intrusions [2–5]. These regions were recognized through a combination of detailed geological mapping and U-Pb zircon geochronology [6,7], whole rock geochemistry [2,8], isotope terrane mapping [9,10], and detailed reconstructions of volcanic-sedimentary facies [11,12]. Once a favorable package of stratigraphy (and/or VMS bearing horizon) has been identified, alteration litho-geochemistry, spectral analysis, and downhole geophysics (particularly electromagnetics), are proven techniques for the effective discovery of massive sulfides [4,13,14]. Regolith and groundwater geochemical anomalies have also been shown to detect some deposits [15–17].

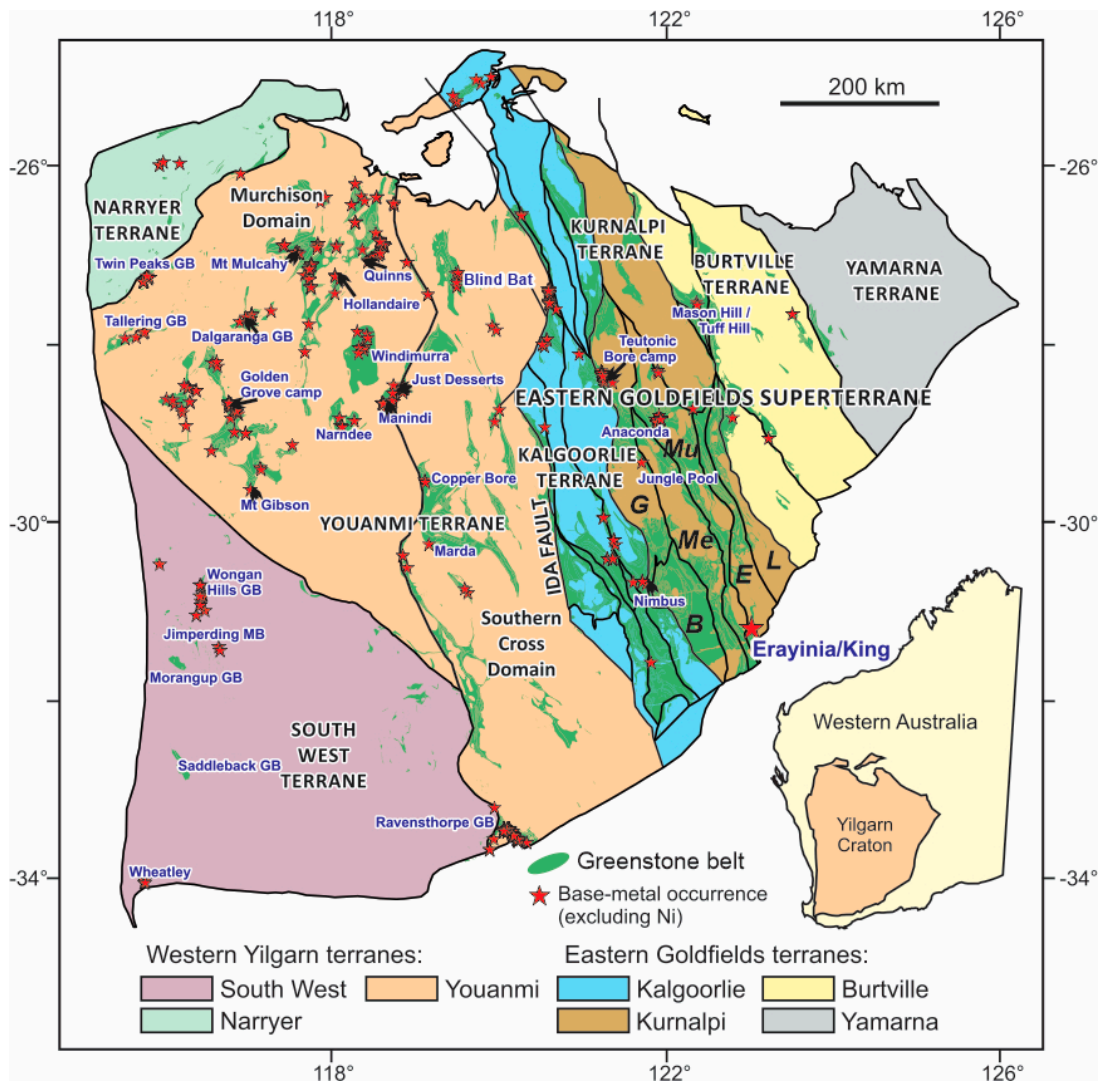


Figure 1. Major terrane and domain subdivisions of the Yilgarn Craton, Western Australia, showing the distribution of greenstone belts and base-metal occurrences (red stars) (modified after [2]). Significant VMS deposits are labeled. Domains: B, Boorara; E, Edjudina; G, Gindalbie; L, Linden; Me, Menangina; Mu, Murrin. Other abbreviations: GB, greenstone belt; MB, metamorphic belt. The Teutonic Bore camp includes the Teutonic Bore, Jaguar, and Bentley VMS deposits.

VMS mineralization in the Yilgarn Craton spans from c. 3.2 Ga to c. 2.68 Ga, with mineralization episodes being terrane-specific and related to regional extension, often following plume magmatism [2]. In the Youanmi Terrane (Figure 1), VMS deposits occur in greenstone belts constrained to: c. 2.97 Ga (e.g., Ravensthorpe), c. 2.95 Ga (Golden Grove camp), c. 2.93 Ga (Mt. Gibson), c. 2.82 Ga (Austin-Quinns, Just Desserts), c. 2.75 Ma (Hollandaire, Dalgara), and c. 2.72 Ga (Altair, Bevan, The Cup) [2–4,11,18,19]. In the Eastern Goldfields Superterrane (EGS), episodes of VMS mineralization have been recognized at c. 2705 Ma (Nimbus and Anaconda deposits), c. 2695 Ma (Teutonic Bore camp), and at c. 2685 Ma (Erayinia NW) [2,5,14,20]. Most major VMS deposits are constrained to broad zones of juvenile crust identified through Sm-Nd isotope mapping of granites, and Pb isotope mapping using galena [9,10]. In the EGS, one such paleo-rift zone is coincident with the Kurnalpi Terrane and was termed the Teutonic zone [9,10].

At Erayinia, in the southeast Kurnalpi Terrane (Figure 1), the emplacement of late granitoids led to the variable metamorphism of greenstone belts up to mid-amphibolite grade. This event significantly impedes the correlation of volcanic units within identified packages of prospective stratigraphy along strike, as well as the identification of mineral assemblages that were associated with primary hydrothermal processes. A small base metal deposit called the King deposit has been recognized (~2.146 Mt at 3.47% Zn, non-compliant) [8]. The host stratigraphy is mineralogically complex, strongly banded, internally faulted, and locally deformed [8]. Due to the small size of the deposit and overturned nature of the stratigraphy, little exploration has occurred either into the hanging-wall or along strike until recent years.

Here, we present results from the King North Zn-Cu-Au prospect, 2.5 km north of the King deposit. Through extensive logging of rock chips, petrography, SEM imaging, XRD analysis, and lithogeochemistry, the King North stratigraphy has been characterized and correlations have been made with the King area. The approach adopted here demonstrates how a robust volcanic stratigraphy can be established through a combination of rock chip logging, petrography, and lithogeochemistry. VMS alteration halos can be recognized across variably metamorphosed and complex volcanic facies.

2. Regional Geology of the Southern Kurnalpi Terrane

The Yilgarn Craton is one of the largest fragments of Archean crust worldwide and records a history of crustal growth from c. 4.4 Ga to 2.6 Ga [20,21]. The craton is composed of Archean granite–greenstone terranes and may be subdivided into a series of terranes and domains based on distinct lithological associations, geochemistry, and ages of volcanism (Figure 1) [22–24]. Here, we focus on the geology of the southern Kurnalpi Terrane around Erayinia.

The Kurnalpi Terrane is characterized by 2.72–2.70 Ga mafic calc-alkaline volcanic complexes (including abundant intermediate rocks) with thin interlayered komatiites [25]. Between 2692 and 2680 Ma, volcanic centers in the Kurnalpi Terrane are associated with largely bimodal (basalt–rhyolite) volcanic rocks and associated sedimentary rocks [25,26]. The Erayinia region is located ~100 km ESE of Kalgoorlie, towards the SE margin of the Kurnalpi Terrane [23]. Three major domains were recognized by Geological Survey of Western Australia (GSWA) mapping [27]: Menangina, Murrin, and Edjudina (Figure 2), of which only the latter is of interest here.

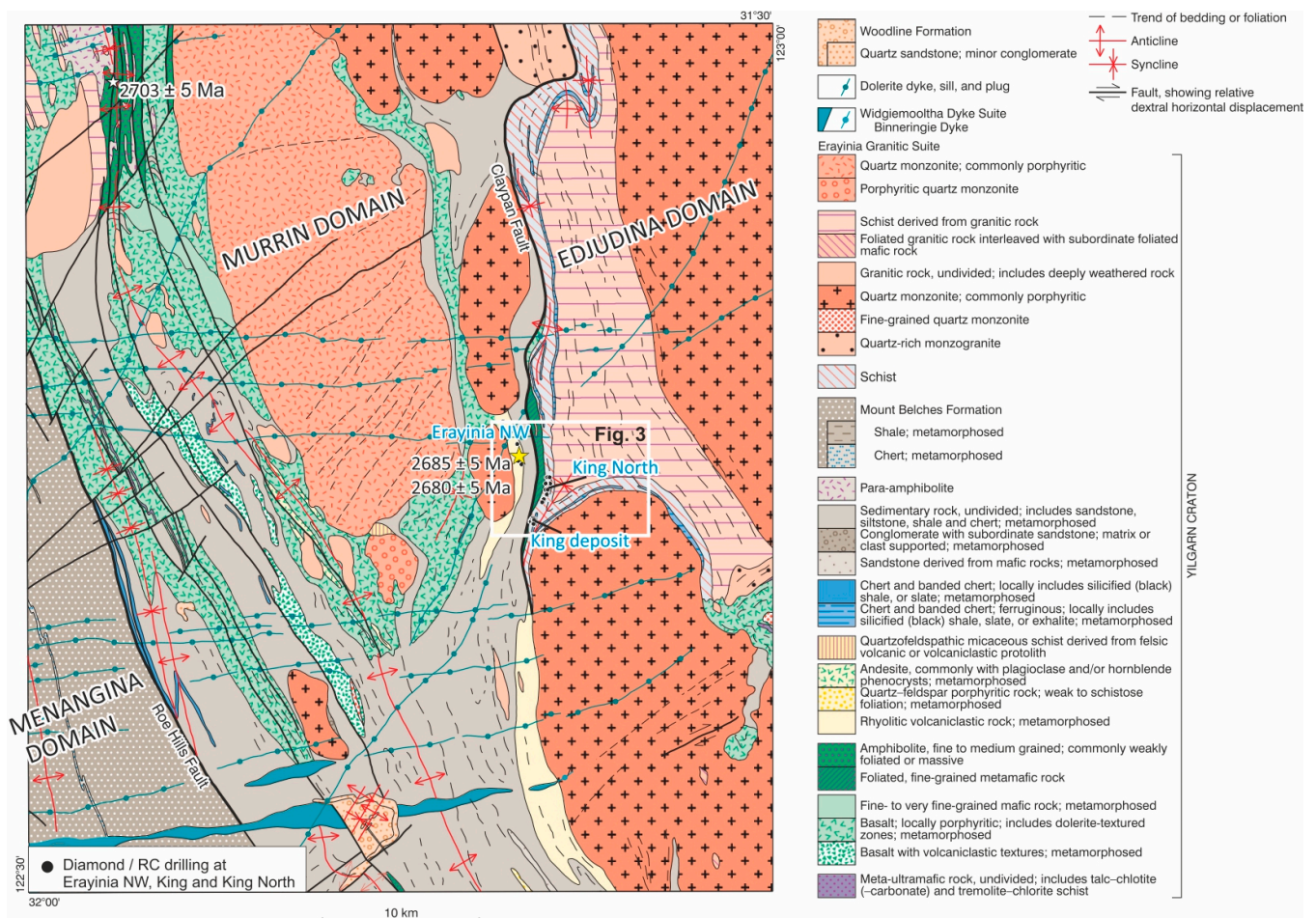


Figure 2. Geological map of the central Erayinia region (modified after [27]), highlighting the position of the King deposit in the Edjudina Domain, east of the Claypan Fault. U-Pb zircon ages (yellow stars) are from [14,28].

The Edjudina Domain, along its ~300 km length, is characterized by tholeiitic basalt, calc-alkaline andesitic volcanic complexes, and minor amounts of komatiite [29]. These rocks are overlain by a laterally extensive belt of epiclastic rocks that are interbedded with horizons of banded iron formation (BIF), chert, and slate, subsequently intruded by doleritic sills [30]. Three U-Pb zircon ages exist for the domain: (i) 2708 ± 6 Ma from a metadacite within a felsic sequence associated with calc-alkaline rocks ~100 km north of King [31], (ii) 2698 ± 10 Ma from a metatonalite at Round Hill, also ~100 km north of King [32], and (iii) 2680 ± 4 Ma from a granite gneiss 30 km NE of King [33].

3. Stratigraphy of the King Deposit

Hollis et al. [8] presented the first account of the stratigraphy hosting the King Zn (-Cu-Au) deposit, which is summarized and expanded upon here based on new petrography and core logging. Formal rock nomenclature has been revised to be consistent with the IUGS Submission on the Systematics of Metamorphic Rocks [34]. The King deposit is overturned, and the local footwall stratigraphy (the K1 package of Figure 3) is characterized by the following units with stratigraphic height: (i) *biotite–muscovite schist*, (ii) *garnet–amphibolite*, with local zones characterized by *magnetite–chlorite schist*, and (iii) a thick package of intermediate to felsic rocks represented by *chlorite–muscovite–quartz schist*, *muscovite–quartz schist*, and *muscovite–chlorite schist* that form the immediate stratigraphic footwall to massive sulfide mineralization. The *muscovite–chlorite schist* (previously termed ‘talc schist’ by company personnel) is interpreted to represent intensely Mg metasomatised intermediate

to felsic volcanic rocks. Relatively thin units of *graphitic schist* also occur in the footwall stratigraphy, though are uncommon. Stringer sulfide mineralization at King occurs as locally intense zones of pyrite (sphalerite) and pyrrhotite–pyrite (–chalcopyrite) veining throughout footwall lithologies, which are recrystallized into the regional foliation.

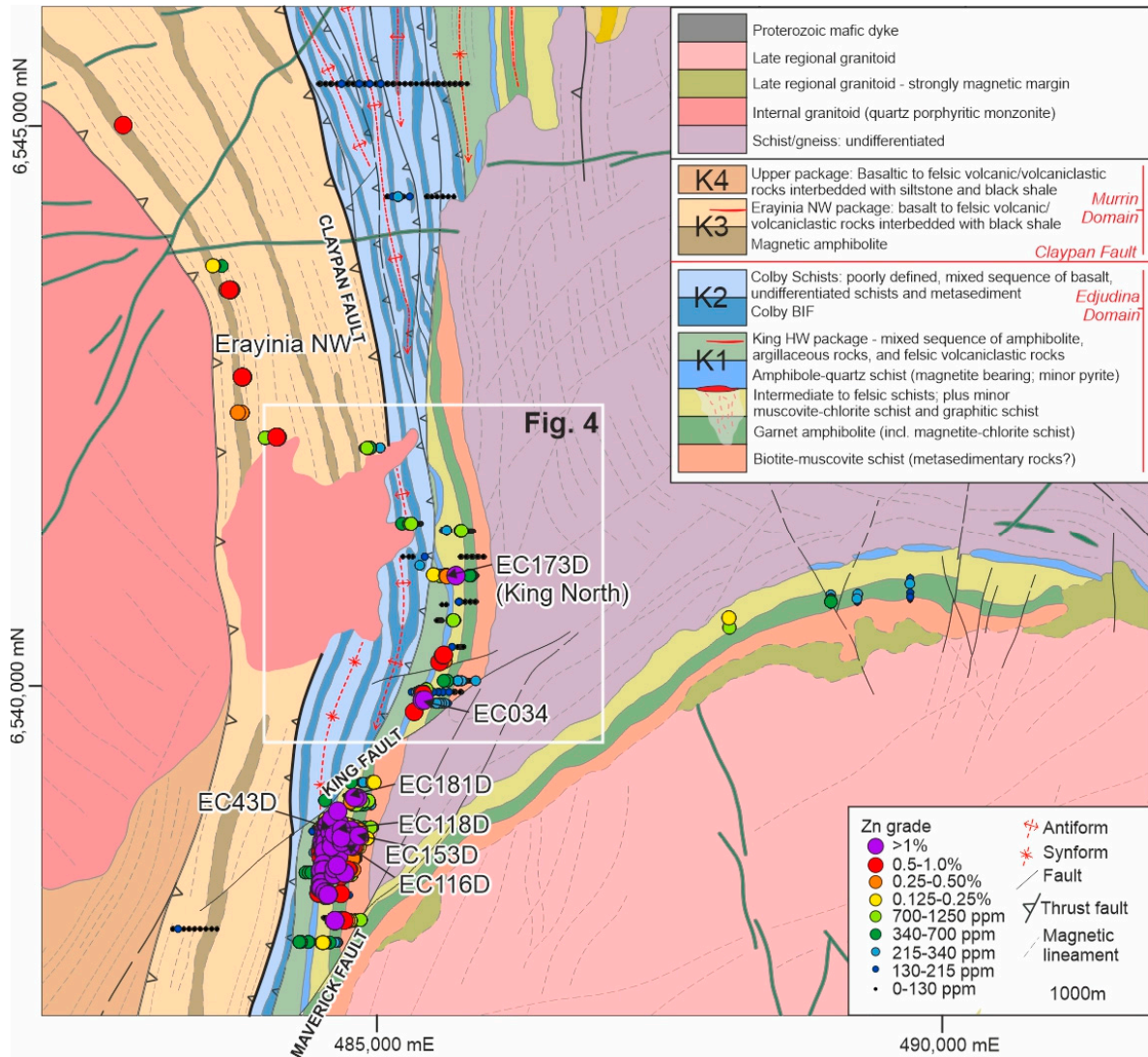


Figure 3. A revised geological map of the Erayinia NW, King and King North areas. This map was derived from integrated GSWA outcrop data, coupled with litho-geochemistry results from regional drilling, and an interpretation of 2018 airborne magnetic data.

Massive sulfide mineralization (1–7 m thick) is characterized by stratiform pyrite–pyrrhotite–sphalerite at the contact between the felsic *muscovite–quartz schists* and a thin unit of *amphibole–quartz schist* (the ‘grunerite-BIF’ of [8]). The latter is interpreted as a metamorphosed exhalite. Overlying hanging-wall lithologies are dominated by argillaceous sedimentary rocks, intermediate to felsic meta-volcaniclastic rocks, and thin units of amphibolite.

4. Exploration History

Over the last ten years (2012–2023) Black Raven Mining has conducted an extensive program of soil and rock-chip geochemistry across the Erayinia area. A heliborne VTEM (Versatile Time Domain EM) geophysical survey was flown in 2013, identifying 24 targets. In late 2018, a high-resolution regional airborne magnetic survey was also flown (10,060 line-kilometers, at 37 m height and 50 m line spacing) to enhance geological map-

ping and facilitate regional correlations of the VMS-favorable stratigraphy [35]. This was complimented by extensive regional aircore (AC), Rotary Air Blast (RAB), and Reverse Circulation (RC) drilling to aid in re-mapping of the greenstone belt within the tenements. A revised geological map for the southern part of the belt is presented in Figure 3. In this paper we focus primarily on the King North target area, ~2.5 km along strike from the King deposit.

At King North, a series of RC holes were drilled in 2015–2016 (Figures 4 and 5) over multi-element soil (Zn-Cu-Pb-Tl-Bi-W-Mo) and VTEM anomalies [36]. These occur within the along-strike extension of the King stratigraphy, through the projected King massive sulfide horizon, and deeper in the footwall (Figure 4). A transect of seven west-dipping holes was focused on a central coincident multi-element soil anomaly (Figures 4 and 5). An additional RC hole dipping 60° E (EC179) was also drilled in this transect, and in 2018 a diamond extension to RC hole EC173 from ~125 to 360 m (termed EC173D; Figure 5a; [35]) was added.

Several zones of base and precious metal mineralization (Figure 5b) have been intersected to date at King North [36], including the following:

- EC175: 24 m at 0.1% Zn and 16 m at 0.3% Cu,
Including 11 m at 0.3% Cu, 0.52 g/t Au, 9 ppm Ag,
- EC179: 18 m at 0.2% Cu, 0.16 g/t Au, 4.6 ppm Ag,
- EC164: 1 m at 4.7% Zn, 2.0% Pb, 0.69 g/t Au, 128 ppm Ag.

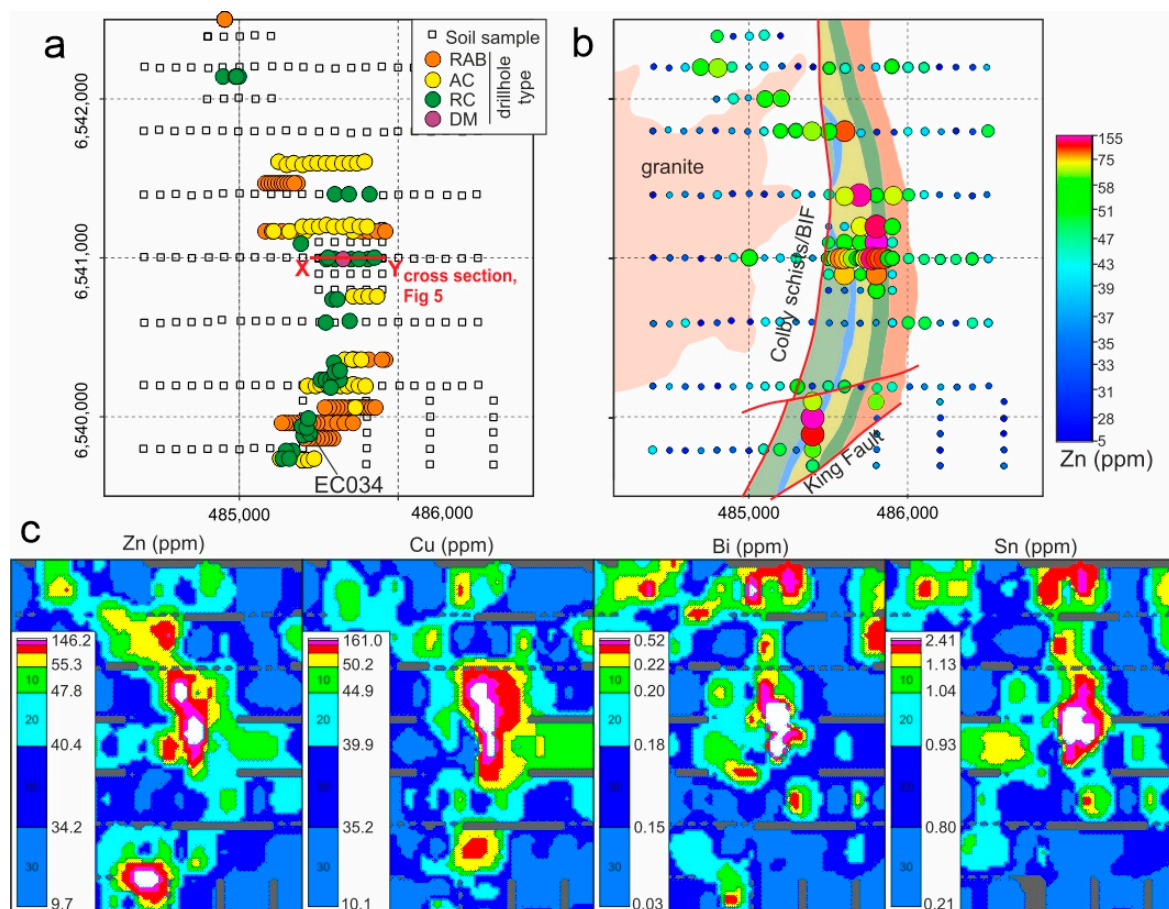


Figure 4. (a) Spatial distribution of soil sampling and drilling at King North. (b) Zn in soil concentrations, shown with the local geology. See Figure 3 for a colour legend. (c) Gridded Zn, Cu, Bi, and Sn soil geochemistry. Colored using unequal bins at 30, 60, 80, 80, 90, 95, 97, 99, and 100% of the data. The location of the central cross section at King North (Figure 5) is shown in Figure 4a.

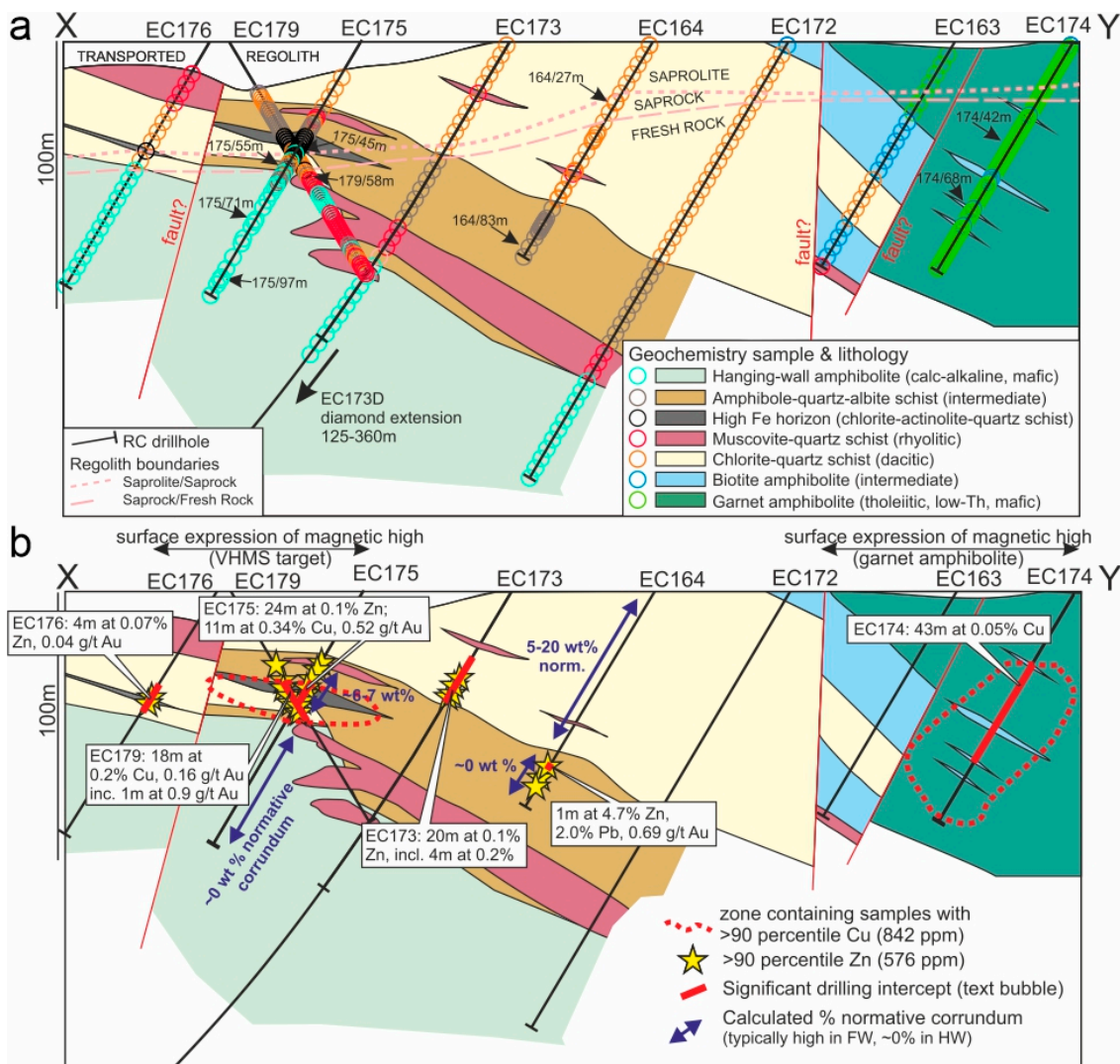


Figure 5. (a) Cross section through the stratigraphy of the King North prospect. Circles represent whole rock geochemistry samples colored according to interpreted lithologies. Pink dashed lines denote regolith boundaries. (b) The same cross section as above, with mineralized intercepts shown and calculated CIPW normative corundum values (after [37]).

5. Methods

To characterize the geology at King North and establish correlations with the King stratigraphy, a suite of samples were collected from several RC and diamond drill holes for petrography, whole rock geochemistry, and X-ray diffraction (XRD) analysis. These included the following: rock chips from holes EC163, EC164, EC174, EC175, and EC179 (Figure 5); diamond drill core from the King North extension hole (EC173D; Figure 5); and diamond drill core from King where the hanging-wall stratigraphy had been intersected (i.e., holes EC181D, EC118D, EC043D; Figure 3).

5.1. Petrography

A suite of polished thin sections were characterized using optical microscopy and by Scanning Electron Microscopy at the University of Southampton (Southampton, UK), and University College Dublin (Dublin, Ireland). In Southampton we used a Zeiss Leo 1450VP SEM and an Oxford Instruments X-Act 10 mm² area SEM-Energy Dispersive Spectrometer (EDS), utilizing the AZtec Energy software system. Semi-quantitative energy dispersive X-ray spectroscopy (EDS) was used on backscatter electron (BSE) images to aid mineral

identification and to classify the alteration mineralogy. In Dublin we used a benchtop Hitachi TM3030Plus Tabletop SEM. Chemical maps were completed over 2–3 h each using a pixel dwell time of 800 ms, resolution of 1024, and process time of 4 s. Composite colour maps were produced by merging element concentration maps of interest using the Oxford Instruments AZtec One (v. 3.2) software (detailed in [8]).

5.2. Whole Rock Geochemistry

Forty-nine samples were analyzed for whole rock geochemistry at ALS Laboratories, Loughrea, Ireland, in two batches. This complements previously published whole rock geochemical data obtained exclusively from the King deposit [8]. Major element concentrations were determined by four-acid digestion with an ICP-OES finish on fused glass beads. Trace element, high field strength element (HFSE), and rare earth element (REE) concentrations were determined by lithium borate fusion and an ICP-MS finish. The base metals (Cu, Pb, Zn, Ni) and trace metals (As, Sb, Tl, Bi) were analyzed by multi-acid digestion, followed by an ICP-OES and an ICP-AES finish, respectively. Lastly, carbon and sulfur were measured by total combustion using a carbon–sulfur analyzer, with loss of ignition (LOI) measured via a robotic thermo-gravimetric system.

Precision (%RSD) and accuracy (%RD) were monitored using laboratory blind, mineralized and unmineralized international standards (OREAS931—Mineralized Siltstone, OREAS24c Basalt). Precision was calculated by repeated analysis of the OREAS931 standard. Whole rock geochemistry results are presented in Supplementary Table S1.

A large geochemical dataset was also provided by Black Raven Mining of rock chips from the King North RC holes (Figure 5a) and diamond core from King (including extensive sampling of core from hole EC153D). This dataset was obtained by four-acid digestion at ALS Laboratories (Perth, Australia) and was used to compliment the high-quality litho-geochemical dataset described above. A more extensive four-acid geochemical dataset was also used by Black Raven Mining, along with the regional airborne magnetic survey, to reinterpret the regional geology (Figure 3).

5.3. X-ray Diffraction

X-ray diffraction (XRD) analysis was performed, using a Philips X'pert pro diffractometer at the University of Southampton, for twenty samples of rock chips from holes EC164 and EC175, which extend from the footwall to interpreted hanging-wall of the VMS prospective horizon. Samples were chosen based on the depth of the sample and a variety of geochemical parameters to provide a representative analysis of each drillhole. Conditions were set to 35 Kev and 40 mA. Quantitative XRD analysis was computed by the software package Siroquant. The results are presented in Supplementary Table S2.

6. Results

6.1. Shallow King North Stratigraphy

The uppermost stratigraphy at King North can be divided into several distinct lithological groupings as shown in Figure 5: (1) an eastern sequence of *garnet amphibolite* (tholeiitic, basaltic affinity) and intermediate *biotite amphibolite*; (2) an upper sequence of *chlorite–quartz schist* of felsic (predominantly dacitic) composition; (3) a mixed sequence of *amphibole–quartz–albite schist* of intermediate composition; and (4) a deeper sequence of *amphibolite* of mafic composition (termed the HW amphibolites). A suite of high-field strength-element-(HSFE-) enriched rhyolitic rocks were also identified and termed the *muscovite–quartz schists*. A narrow unit of *chlorite–actinolite–quartz schist* occurs around Zn mineralization and is interpreted as a meta-exhalite (Figure 5). Each package is described separately. Representative petrographic images are presented in Figure 6.

Garnet amphibolite (basaltic): these units were intercepted in the easternmost RC holes (Figure 5). Rock chips are dark green in colour with a strong foliation. Large pink garnet porphyroblasts (to ~0.5 cm; ~20% of rock) are heavily fractured and filled by a mixture of quartz and chlorite (Figure 6a). The remainder of the rock is dominated by a

foliated groundmass of large crystals of actinolite (35%), chlorite (30%), quartz (10%), and disseminated sulfides (<5%, predominantly pyrite and pyrrhotite, lesser chalcopyrite). The sequence is interpreted as a thick package of mafic volcanic or volcanoclastic rocks.

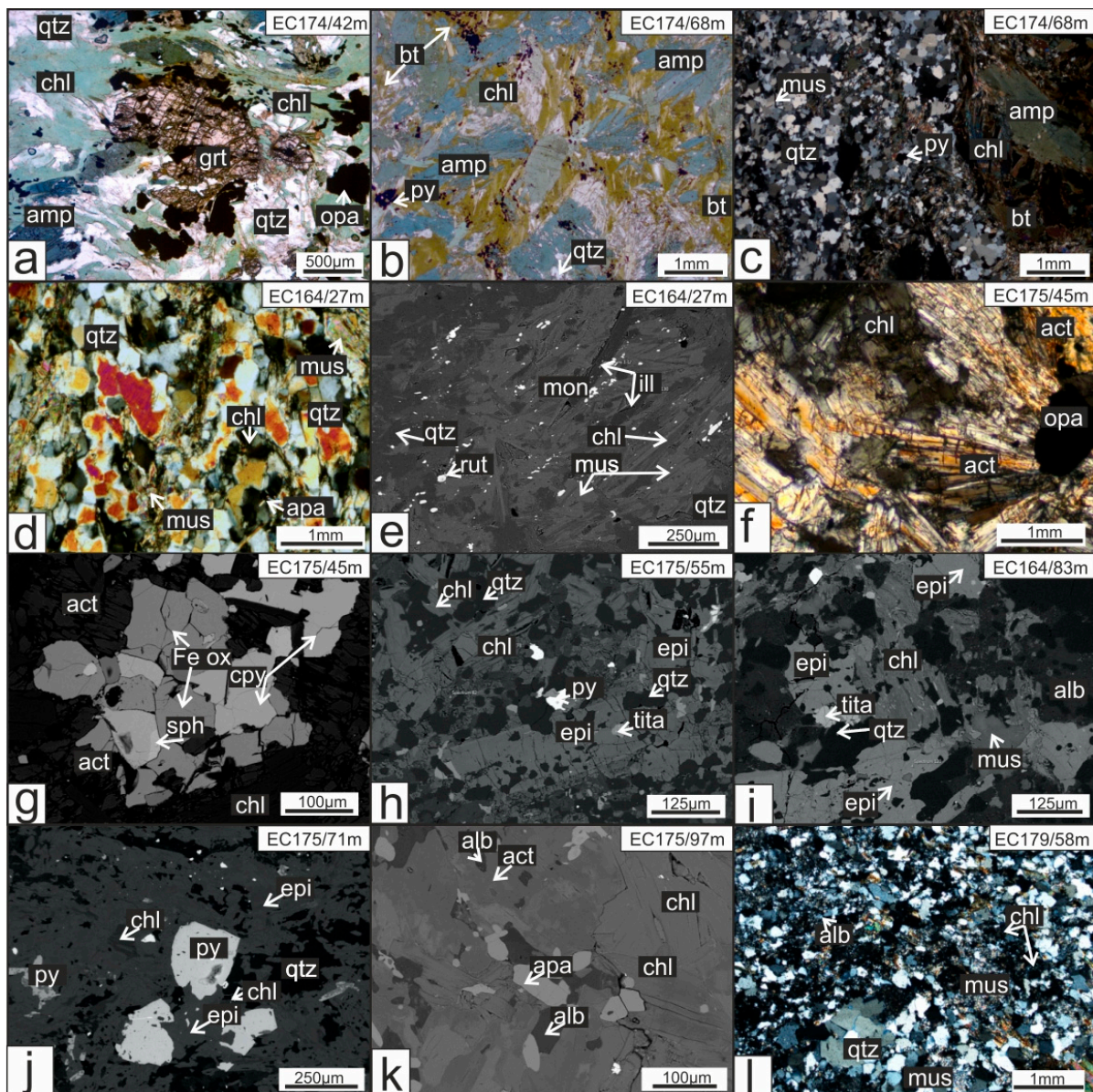


Figure 6. Petrography of key lithologies identified from rock chips at King North. (a) Garnet amphibolite. Fractured garnet porphyroblasts are filled by chlorite and quartz, and surrounded by actinolite, chlorite, quartz, and sulfides. (b,c) Biotite amphibolite. Strongly layered with domains either dominated by actinolite and biotite or recrystallized quartz. (d,e) Chlorite–quartz schist. Abundant recrystallized quartz with lesser chlorite and minor muscovite. (f,g) Chlorite–actinolite–quartz schist. Dominated by actinolite and chlorite with disseminated magnetite, sphalerite, and chalcopyrite. (h,i) Amphibole–quartz–albite schist. Highly variable mineralogy, with large epidote crystals occurring in some samples, and surrounded by albite, quartz, amphibole, and minor muscovite. (j,k) Hanging-wall amphibolite. Characterized by actinolite, albite, chlorite, epidote, and quartz. (l) Muscovite–quartz schist. Contains abundant recrystallized quartz, with lesser muscovite and minor chlorite and albite. Sample locations are shown in Figure 5a. *Mineral abbreviations:* act, actinolite; amp, amphibole (unknown type); alb, albite; apa, apatite; bt, biotite; chl, chlorite; cpy, chalcopyrite; epi, epidote; Fe-ox, Fe-oxides; grt, garnet; ill, illite; mus, muscovite; opa, opaque phase; qtz, quartz; rut, rutile; sph, sphalerite; tita, titanite. *Image type:* transmitted light, (a,b); polarized light, (c,d,f,l); SEM, (e,g,k).

Biotite amphibolite (andesitic): the garnet amphibolite is interbedded with a biotite-rich amphibolite of intermediate composition in hole EC174 that becomes the dominant lithology with depth in hole EC163 (Figure 5). The biotite amphibolite is composed of approximately equal portions of actinolite (40%) and biotite (40%) (Figure 6b,c), with large clots and segregations (15%) dominated by recrystallized quartz that contain minor patches of green amphibole, muscovite, biotite, and small actinolite needles. Sulfides (~5%) are disseminated throughout along the main foliation. The sequence is interpreted to represent a package of intermediate volcanoclastic rocks.

Chlorite–quartz schists (dacitic): within the upper parts of each western RC drillhole at King North, samples contain abundant fine quartz (XRD: ~62%–90%), with intergrowths of chlorite (~8%–27%) and muscovite (~1%–10%) (Figure 6d). Muscovite is being partially replaced by chlorite in patches. Relict plagioclase (albite) is rare (Supplementary Table S1), and when present retains its twinning. SEM imaging revealed the presence of illite within the groundmass. Minor rutile, apatite, zircon, and monazite were also identified by SEM (Figure 6e). The mineralogy indicates a quartzo-feldspathic protolith of dacitic composition. They are interpreted to represent a thick sequence of weakly metamorphosed dacitic volcanic and volcanoclastic rocks.

Muscovite–quartz schists (dacitic to rhyolitic): geochemical data reveal several narrow intervals characterized by high Zr/TiO₂ ratios and concentrations of the high-field-strength elements (HFSE), predominantly within the dacitic package of chlorite–quartz schists and deeper amphibole–quartz–albite schists (Figure 5). These were identified mainly from holes EC174 and EC179, with thinner units also subsequently recognized in holes EC163, EC164, and EC172 (Figure 5). These foliated rocks are dominated by recrystallized quartz (~60%), feldspar replaced by muscovite (~25%), and chlorite (~10%), plus minor amounts of pyrite (~5%). Some samples drilled below the chlorite–actinolite–quartz schist also contain minor albite (Figure 6l). They are interpreted to represent high-level intrusive sills, or thin packages of rhyolitic volcanoclastic rocks.

Chlorite–actinolite–quartz schist (high-Fe unit; exhalite): in drillhole EC175, from 38 to 47 m a thin and petrologically distinct unit was identified that is associated with very high Fe₂O₃ (>25 wt%) and variable S (3 to >10%) contents, associated with Cu–Au mineralization (Figure 5: 11 m at 0.3% Cu, 0.52 g/t Au). Equivalent units occur in holes EC179 and EC176, directly to the west. The rock is strongly weathered, occurring near the saprolite/saprock boundary, and is dominated by bands of actinolite and chlorite, with abundant disseminated magnetite and recrystallized quartz. Actinolite occurs as elongated, splinter-shaped crystals often radiating out from the magnetite grains (Figure 6f,g). Chlorite dominates the groundmass in the mafic bands. Disseminated cubes of pyrite are present as the dominant sulfide, along with sphalerite and chalcopyrite (Figure 6g).

Amphibole–quartz–albite schists (andesitic): below the felsic rocks in each RC drill-hole, a mineralogically variable sequence of coarse-grained schists of intermediate composition occur (Figure 5). XRD analysis of selected rock chips reflected either coarse clinzoisite crystals (e.g., 44% epidote) or the finer groundmass, which is dominated by albite (24%–49%), quartz (20%–41%), amphibole (absent to 19%), chlorite (10%–21%), and minor muscovite (1%–2%) (Figure 6h,i; Supplementary Table S1). Large epidote crystals are often fragmented. The sequence is interpreted to include a mixed sequence of metasedimentary and lesser volcanoclastic rocks of broadly andesitic composition.

Hanging-wall amphibolites (basaltic–andesitic): directly below the amphibole–quartz–albite schists, the stratigraphy at King North is dominated by amphibolite of mafic composition (i.e., low Zr/TiO₂). These rocks consist of elongated, bladed actinolite (17%–80%), with albite (16%–50%), chlorite (3%–47%), epidote (1%–14%), and interstitial quartz (typically <20%) (Figure 6j,k). Minor amounts of apatite, titanite, pyrite, sphalerite, and chalcopyrite were also identified. Areas of increased quartz–epidote alteration occur towards the base of hole EC164 at 83 m. Together, these rocks represent a sequence of metamorphosed mafic volcanic rocks and/or possible coeval sills.

Sulfide assemblages: the primary sulfide assemblage at King North is dominated by pyrite, sphalerite, chalcopyrite, pyrrhotite, and galena (Figure 6). Sulfides were observed throughout the footwall lithologies as disseminated grains and as stringer veins recrystallized into the regional foliation. With stratigraphic height, the sulfide assemblage transitions from one dominated by pyrite–chalcopyrite–pyrrhotite in the garnet amphibolite, to having increased abundances of sphalerite, galena, and less chalcopyrite in more felsic lithologies (Figure 5). Significant intercepts of base metal mineralization from King North are plotted on the Cu–Zn–Pb VMS ternary diagram [38–41] in Supplementary Figure S1, along with analyses of massive sulfides from the King deposit. Samples from both localities plot predominantly as Zn–Cu- and Zn–Pb–Cu-rich. The central area of King North (Figure 5) is characterized by higher Cu/Zn ratios than the stratigraphy to the south around hole EC034 (Figure 4a).

6.2. Deep King North Stratigraphy

A continuation of the King North stratigraphy is presented as a geological log for the diamond tail of drillhole EC173 in Figure 7. Representative core photos and photomicrographs are shown in Figures 8 and 9, respectively. Graded bedding observed in core from EC173D is consistent with the overturned nature of the stratigraphy. With depth (i.e., increased stratigraphic height), the lithologies encountered are as follows:

Hanging-wall amphibolites (basaltic–andesitic): the top of the diamond tail to EC173 is reflected by the presence of ~100 m of green–dark grey foliated amphibolite, with narrow horizons of mafic schist (Figure 7). This sequence most likely represents a continuation of the same lithologies noted towards the base of the RC drillholes, described above under *hanging-wall amphibolites*. Unlike in the rock chips, subtle distinctions are apparent between porphyroblastic and non-porphyroblastic varieties (Figure 8a,b). Large amphibole porphyroblasts have been largely replaced by chlorite and quartz, in a matrix now dominated by amphibole, plagioclase (albite and oligoclase), chlorite, quartz, and lesser apatite (Figure 9a,b). Minor amounts of actinolite were also identified. Locally intense quartz–epidote alteration is often present around thicker units of intrusive quartz–feldspar porphyry (Figures 7 and 8b). Pyrite stringers occur throughout sections of the core, with some horizons containing minor blebs of chalcopyrite.

Upper mixed felsic volcanoclastic and metasedimentary rocks: directly below the amphibolite sequence is a mixed package (Figure 7: 225–320 m) of the following: (i) intensely silicified and schistose ‘quartz-eye’ felsic volcanic and volcanoclastic rocks (Figure 8d,f), (ii) narrow horizons of muscovite–chlorite schist (Figures 8e and 9h), and (iii) relatively thick sequences of fine-grained metasedimentary rocks. The quartz phenocrysts within the felsic volcanoclastic rocks are either deformed and internally strained or completely recrystallized, surrounded by a matrix of quartz, muscovite, and albite, with minor amounts of calcite, pyrite, and/or pyrrhotite (Figure 9c,d). Rare units preserve internal grading of quartz–albite-rich layers and are crosscut by thin carbonate veinlets (Figure 9e). Some of the felsic units are interbedded with the fine-grained, quartz- and chlorite-rich metasedimentary rocks. The latter contain soft-sediment deformation features and abundant pyrite–pyrrhotite-rich layers (Figures 8g and 9f).

Graphitic schist: rare thin horizons of graphitic schist (Figure 8c) occur with the mixed package of felsic volcanic and fine-grained metasedimentary rocks. The graphitic units are frequently associated with faulting (e.g., Figure 7, 221 m), as in the King stratigraphy [8].

Amphibole–quartz schist (upper meta-exhalite): the package of mixed schists is directly overlain by a <2 m thick amphibole–quartz schist (Figure 8h), and is surrounded by a thick sequence of silica–epidote-altered garnet-bearing amphibolites (Figures 7 and 8i). The amphibole–quartz schist (Figure 7 at 340 m) is characterized by alternating layers dominated by quartz (with lesser muscovite) and amphibole of unknown composition, and contains around 5% disseminated magnetite (Figure 9g).

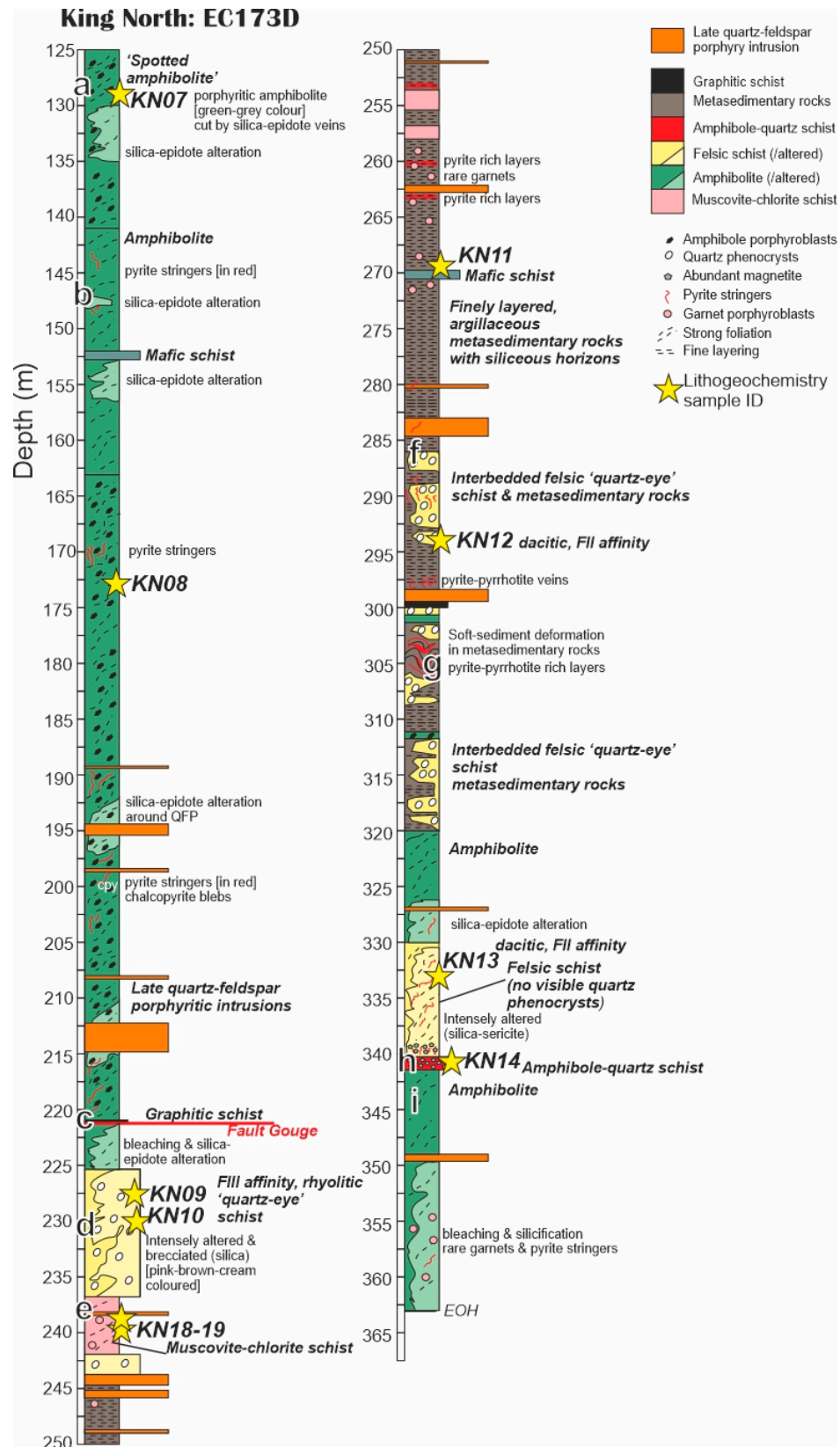


Figure 7. Summary geological log of diamond drillhole EC173D through the King North hanging-wall stratigraphy. Letters a–i correspond to core photographs in Figure 8. Samples analyzed for whole rock geochemistry are indicated. EOH, end of hole.

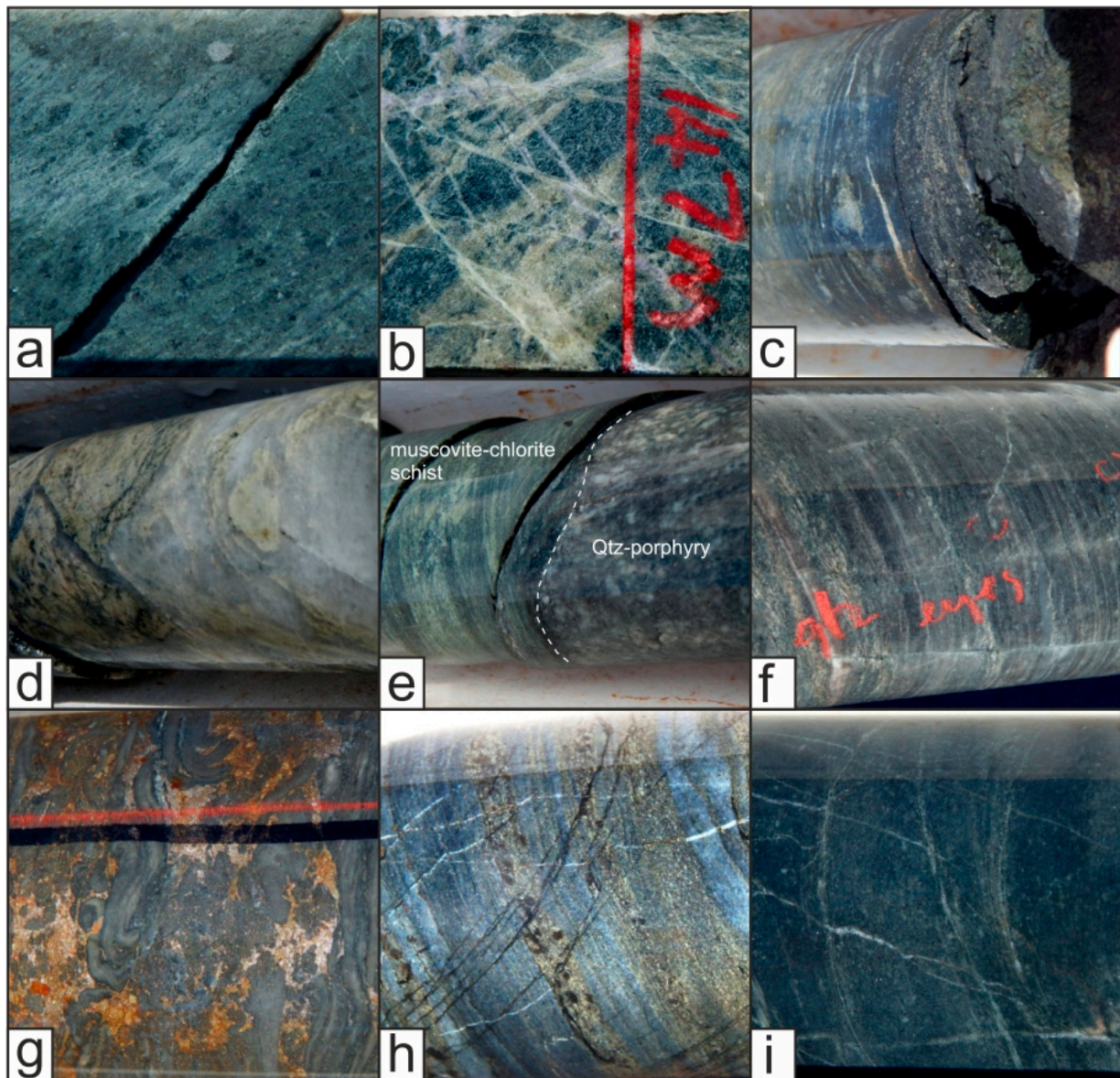


Figure 8. Representative core photographs of key lithologies from EC173D at King North. (a) Amphibolite containing large amphibole porphyroblasts partially replaced by quartz and chlorite. (b) Silica–epidote-altered amphibolite. (c) Narrow unit of graphitic schist. (d) Hydrothermally altered felsic schist (HFSE-enriched), dominated by quartz and muscovite. (e) Late quartz–porphyry intrusion cutting muscovite–chlorite schist. (f) Felsic schist with small, recrystallized quartz eyes. (g) Fine-grained metasedimentary rocks showing soft-sediment deformation features and containing abundant pyrrhotite. (h) Amphibole–quartz schist, an interpreted meta-exhalite. (i) Non-porphyroblastic amphibolite.

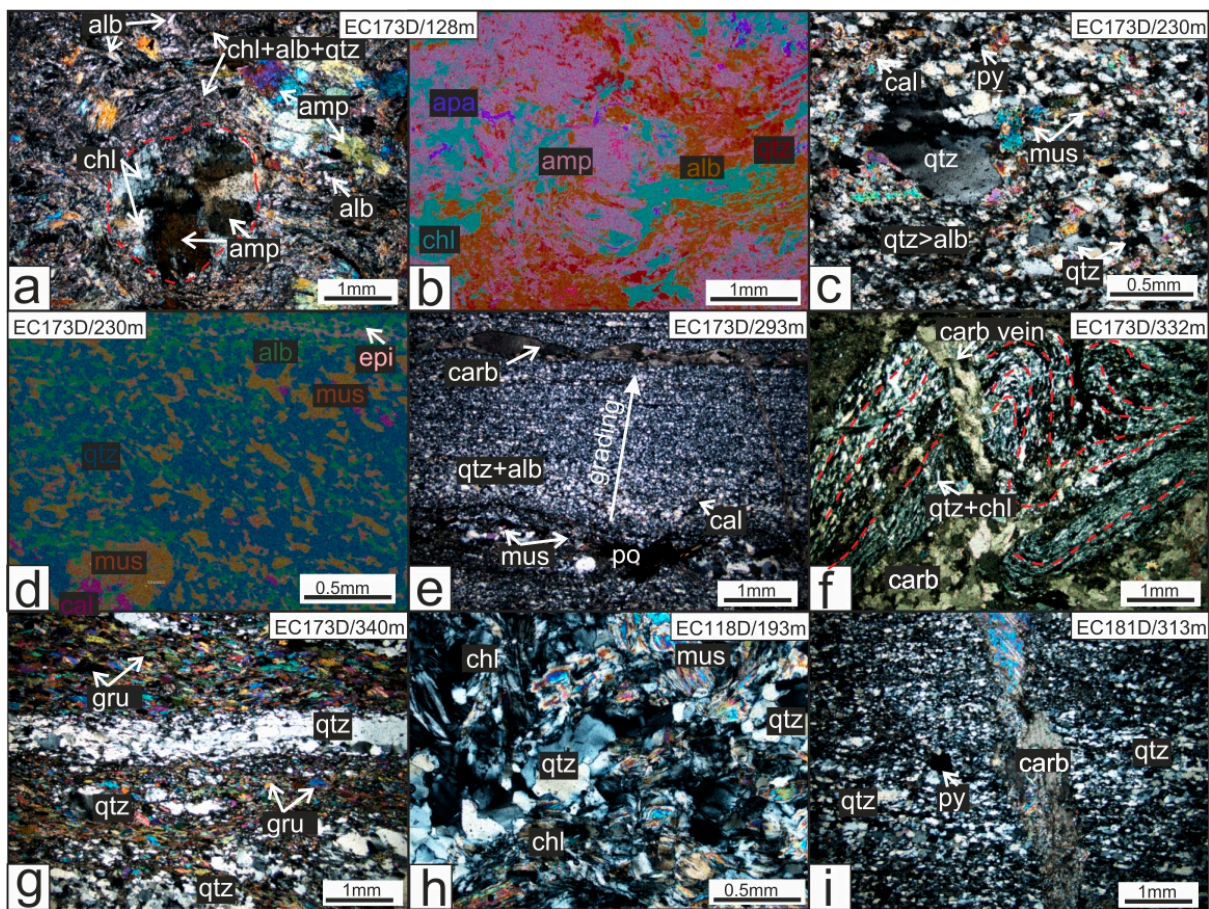


Figure 9. Petrography of key lithologies from diamond drillhole EC173D at King North and other units discussed in the text. (a,b) Amphibolite containing porphyroblasts partially replaced by quartz and chlorite. (c,d) HFSE-enriched albite–muscovite–quartz schist of rhyolitic composition. (e) Sulfide bearing muscovite–quartz schist of dacitic composition with preserved grading and carbonate veins. (f) Soft-sediment deformed sedimentary rocks cut by late carbonate veins. (g) Layered amphibole–quartz schist. (h) Muscovite–chlorite schist with clots and segregations of quartz. (i) Felsic schist with disseminated pyrite, cut by late carbonate veins. *Mineral abbreviations:* amp, amphibole; alb, albite; cal, calcite; carb, carbonate; chl, chlorite; epi, epidote; grt, garnet; gru, grunerite; mus, muscovite; qtz, quartz. *Image type:* polarized light, (a,c,e–i); SEM chemical map, (b,d).

6.3. King North Lithogeochemistry

During hydrothermal alteration, a number of major and trace elements (e.g., Si, Na, Ca, Sr) can become mobile [42,43]. Therefore, common geochemical discriminants, such as SiO₂, MgO, and CaO, cannot be used to identify precursor rock type and magmatic affinity for intensely altered rocks [42]. Only elements that are demonstrably immobile to these processes were used here to characterize magma affinity [42,44]. The discriminants used were as follows: Al₂O₃, TiO₂, Th, Co, V, Nb, Hf, Ta, Y, and Sc, as well as the REE (±Ce, Eu). Chondrite-normalized REE ratios (La/Sm_{CN}, Gd/Yb_{CN}) are after Boynton [45].

Mobile elements were used to characterize the type and intensity of hydrothermal alteration. A number of well-established alteration indexes have been used. The Ishikawa alteration index (AI) quantifies the intensity of chlorite and sericite alteration that occurs within footwall strata to VMS deposits [46]. The chlorite–carbonate–pyrite index (CCPI) measures the increase in MgO and FeO associated with Mg–Fe chlorite development that commonly replaces albite, K-feldspar, or sericite, and the corresponding losses in Na₂O and/or K₂O [47,48]. Plotting these two indexes against each other produces the alteration box plot [48], defining several key alteration trends.

Geochemical data from King and King North are plotted in Figures 10–12. Data from the King deposit stratigraphy include that previously published [8], complimented by new analyses from holes EC153D, EC181D, and EC043D (Figure 13). Here we characterize the geochemical characteristics of the King North sequence. Units are described in stratigraphic order from the base of the volcanic pile, assuming an overturned stratigraphy.

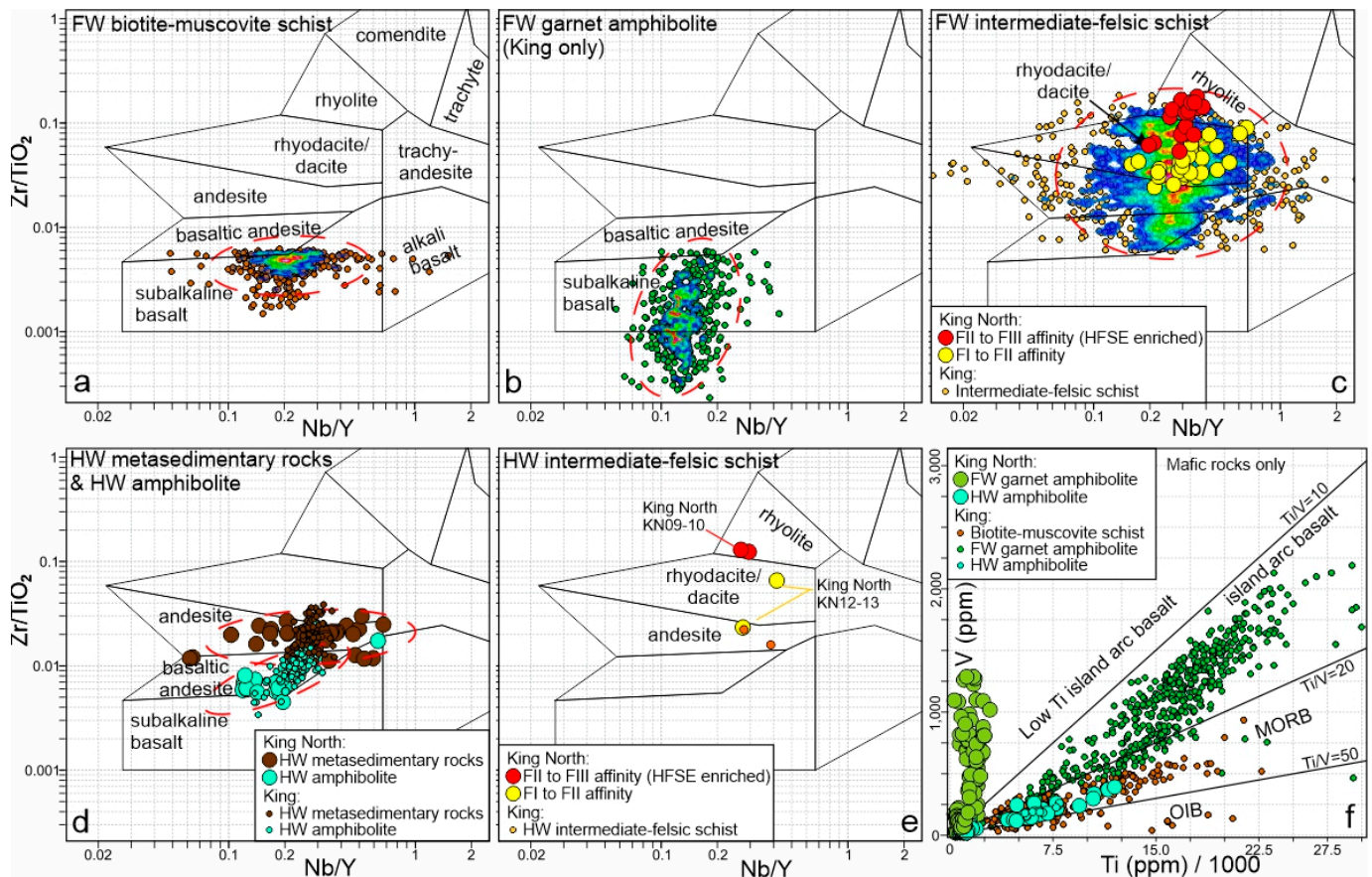


Figure 10. Immobible element geochemistry of key lithologies from the King and King North stratigraphy, divided into those stratigraphically below and above the ore-equivalent horizon. (a) FW biotite–muscovite schist. (b) FW garnet–amphibolite. (c) FW intermediate to felsic schists (i.e., biotite amphibolite, chlorite–quartz schist, chlorite–muscovite–quartz schist, muscovite–quartz schist). (d) HW amphibolite and HW metasedimentary rocks (i.e., amphibole–quartz–albite schists at King North). (e) HW intermediate to felsic schists. Discrimination diagram for (a–e) after Winchester and Floyd [49]. (f) Mafic Ti–V discrimination diagram of Shervais [50]. Dashed red circles represent Mahalanobis ellipses for each lithology ($p = 0.95$). Heat maps reflect point density grids for data-rich lithologies. FW, footwall; HW, hanging-wall.

Garnet amphibolite (basaltic): these rocks are easily distinguished by their very low Ti/V ratios and plot predominantly within the island arc tholeiitic field of the Th–Co discrimination diagram [51] due to their low Th contents (0.13–1.77 ppm) (Figure 11a). Sc contents are also low (typically ~ 10 ppm), but Cr (2–361 ppm) and Co (2–248 ppm) contents are extremely variable. These rocks are otherwise geochemically similar to the garnet amphibolite at King along strike [8], which is associated with disseminated and stringer pyrite–pyrrhotite–chalcopyrite mineralization and local zones of abundant chlorite and magnetite (Figure 14a).

Major elements show large ranges for MgO (0.2–5.9 wt%), CaO (<0.05–5.6 wt%), and Fe₂O₃ (6.4–28.6 wt%). Na₂O, K₂O, and S contents are typically below 1 wt%. On the box plot of Large et al. [48], analyses form a linear trend between Mg–Fe carbonate-altered basalt to the chlorite–pyrite (–magnetite) mineral node (Figure 11c). Metals and VMS-

associated pathfinder elements that are strongly correlated (Spearman Rank method, here and thereafter) include the following: Au-Ag-Cu (0.88–0.63), Mo-Sb (0.55), Zn-Pb (0.54), and Bi-W (0.51). Zones of significant Cu enrichment occur on the central drilling line and closer to the King Fault (Figure 14b).

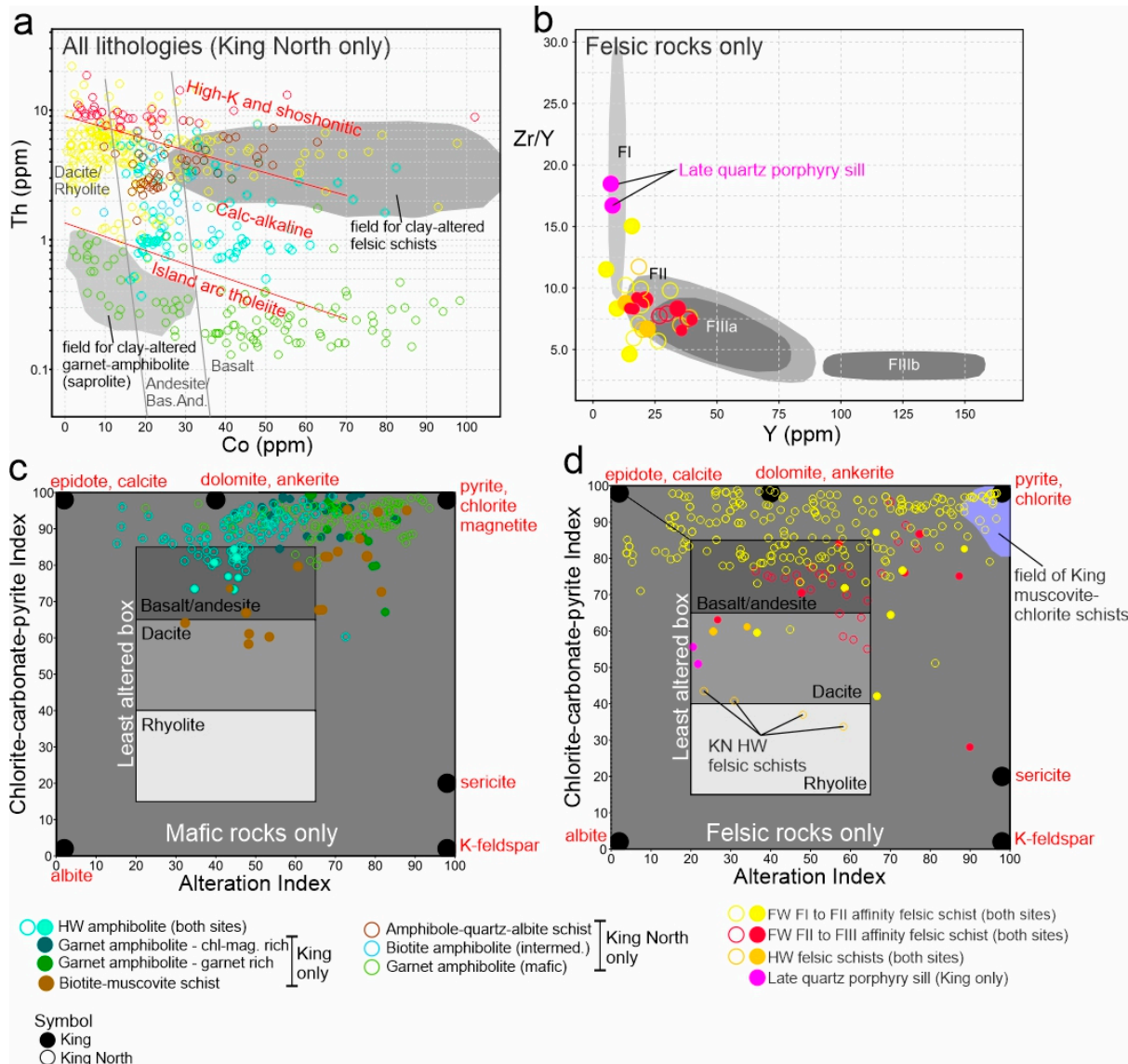


Figure 11. (a) Geochemistry of samples analyzed from King North, plotted on the Th–Co discrimination diagram of Hastie et al. [51] (b) Felsic rocks from King and King North plotted on the VMS fertility diagram of Leshner et al. [52] (c,d) Mafic and felsic rocks plotted on the box plot of Large et al. [48].

Biotite amphibolite (intermediate): the biotite amphibolite drilled in the eastern RC holes is of intermediate composition and calc-alkaline affinity (Figure 11a). These rocks contain significantly higher Th (average ~1.7 ppm, to 6.3 ppm) and lower Co (average ~25 ppm) than the closely associated garnet amphibolites, but have similar Ti/V ratios. Geochemically similar rocks have been identified at King in the footwall, though these are mineralogically distinct [8].

Samples of biotite amphibolite plot on a near identical trend to the garnet amphibolites on the box plot (not shown). MgO, Al₂O₃, K₂O, Na₂O, and S ranges are also similar, though Fe₂O_{3T} contents are notably lower (typically <10 wt%). Trace metal contents are very similar to the stratigraphically underlying garnet amphibolite, though more elements are strongly correlated, including the following: Zn with Pb-Au-Ag and Cu with Au-Ag-Bi-Sn-Te-Tl.

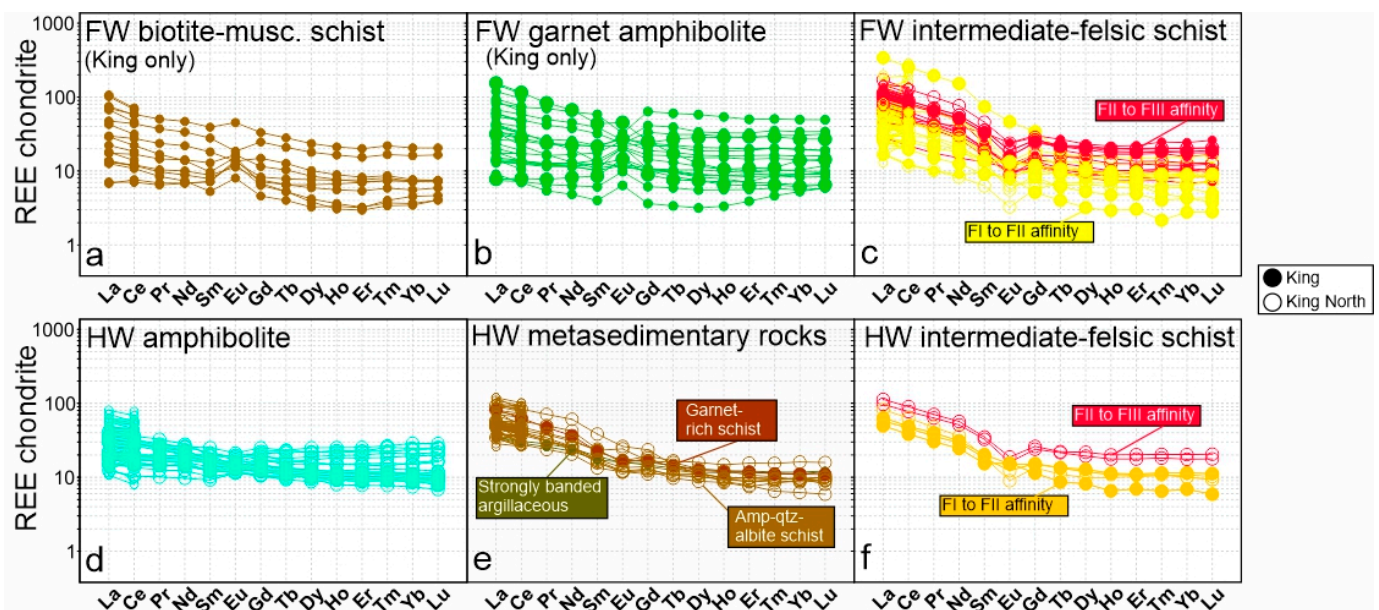


Figure 12. Chondrite-normalized REE spider diagrams (after Boynton [45]) for: (a) FW biotite–muscovite schist, (b) FW garnet amphibolite (King), (c) FW intermediate to felsic schists (i.e., biotite amphibolite, chlorite–quartz schist, chlorite–muscovite–quartz schist, muscovite–quartz schist), (d) HW amphibolite, (e) HW metasedimentary rocks (i.e., amphibole–quartz–albite schists at King North), (f) HW intermediate to felsic schists. Open circles are samples from King North, filled circles are samples from King.

Chlorite–quartz schists (dacitic): extensive lithogeochemical data are available for the chlorite–quartz schists intercepted in RC drilling (Figures 10c and 11a). The rocks plot within the rhyodacite/dacite field of the Winchester and Floyd [49] discrimination diagram due to high Zr/TiO₂ ratios (Figure 10c). These schists are of calc-alkaline affinity (Zr/Y 5.7–10.2; ~6 ppm Th; Figure 11a) have moderately dipping chondrite-normalized LREE profiles (La/Sm_{CN} 2.7–4.0), gently dipping to flattish HREE profiles (Gd/Yb_{CN} 0.9–1.9) and generally small negative Eu anomalies (Figure 12c). They plot predominantly in the FII classification field of Lesher et al. [52] (Figure 11b). They are closely associated with FIII-affinity high-Zr/Ti rhyolites (Figure 5), which are discussed below (the muscovite–quartz schists) and are geochemically identical to the immediate felsic footwall sequence hosting the King deposit (Figures 10c and 12c; [8]).

The chlorite–quartz schists have variable SiO₂ (typically 75–85 wt%), low CaO (<0.4 wt%), very low Na₂O (often <0.25 wt%), and notably lower Fe₂O_{3T} (typically ~3 wt%) than both the biotite amphibolites and garnet amphibolites. One sample (EC164: 62–63 m) was associated with very high MgO (17.25 wt%) and low SiO₂ (42.1 wt%), possibly due to intense chloritization. On a box plot, the chlorite–quartz schists of King North are nearly all characterized by high CCPI and occupy a trend from carbonate alteration to intense pyrite–chlorite alteration (Figure 11d). Three notable groups are identifiable in metal correlations: Au–Ag, Zn–Ni, and Bi–Cu–Pb–Sb–Te±Mo±Sn±Tl. Antimony and Cd contents are significantly higher in the felsic schists than those described above. Tellurium contents reach 5 ppm. Significant zones of Zn enrichment can be traced along the contact between this rock type and overlying amphibole–quartz–albite schists (Figure 5). In the western RC drill holes this unit is stratigraphically underlain by a zone of anomalously high (>90 percentile) Cu (Figure 5).

Muscovite–quartz schists (dacitic to rhyolitic): these rocks straddle the rhyodacite and rhyolite fields of the Winchester and Floyd [49] diagram due to significantly higher Zr/TiO₂ ratios (Figure 10c). They also contain higher REE content than associated dacitic rocks (Figure 12c), similarly flat HREE profiles (Gd/Yb_{CN} 1.3–2.2), and are of FIII affinity

according to the rhyolite fertility diagram of Leshner et al. [52] (Figure 11b). High Th concentrations (>7 ppm) place the rocks on the high-K/shoshonitic trend of Hastie et al. [51], whereas the FII rocks described above are of calc-alkaline affinity (Figure 11b). Equivalent rocks were not recognized in the King stratigraphy by Hollis et al. [8] but have since been identified using a larger lithogeochemical company dataset.

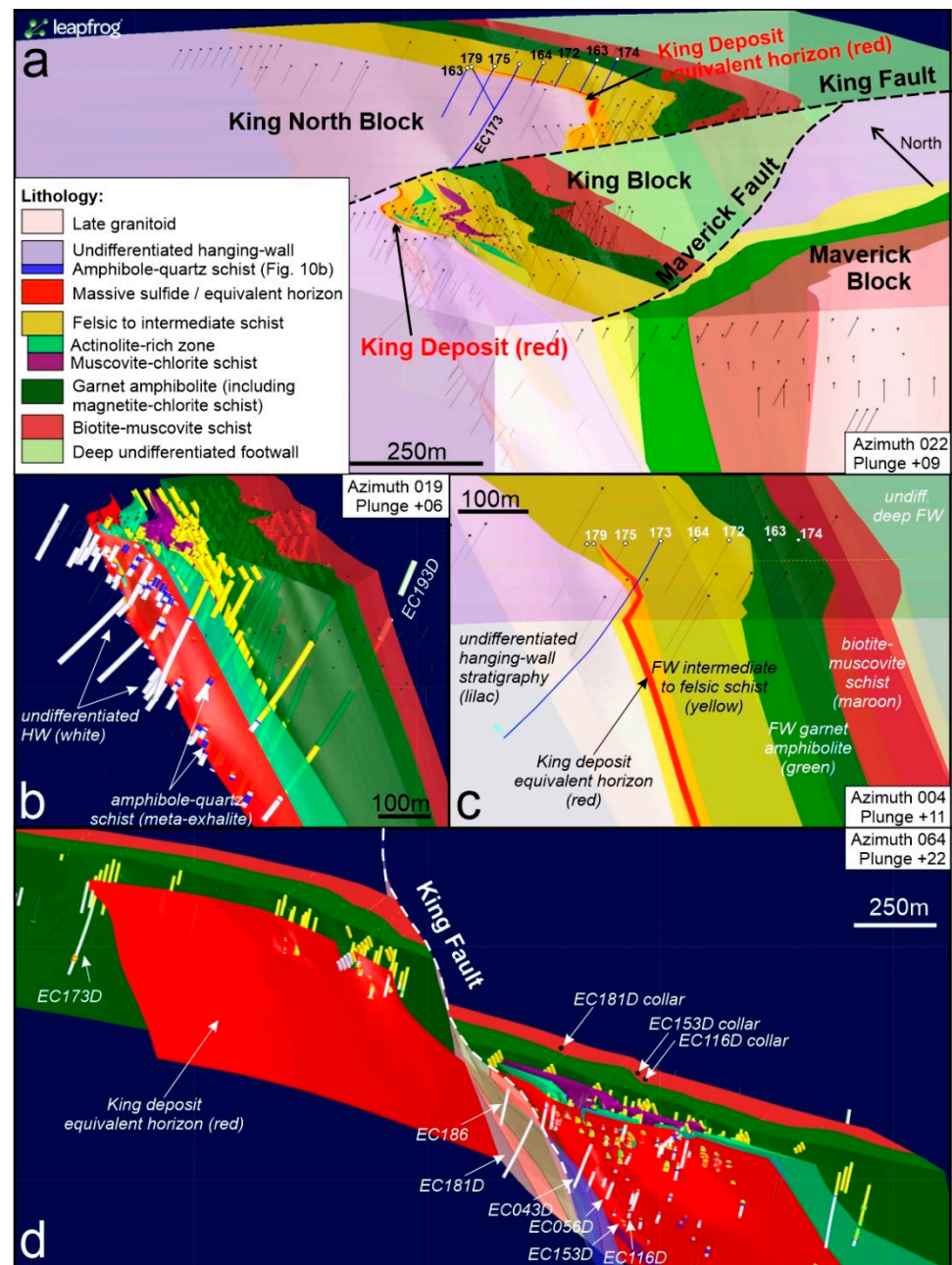


Figure 13. (a) Leapfrog block model showing the segmentation of the King regional stratigraphy into the King, King North, and Maverick blocks. (b) Major lithological units within the King deposit. Note the thin unit of amphibole–quartz schist (blue) in the immediate stratigraphic hanging-wall to massive sulfide mineralization, and the muscovite–chlorite schist (purple) in the central footwall. (c) Slice through the central area at King North highlighting the extent of hole EC173D into the stratigraphic hanging-wall. (d) Leapfrog model showing the offset of key geological units and the ore equivalent horizon due to the King Fault. Key drillholes discussed in the text are labeled.

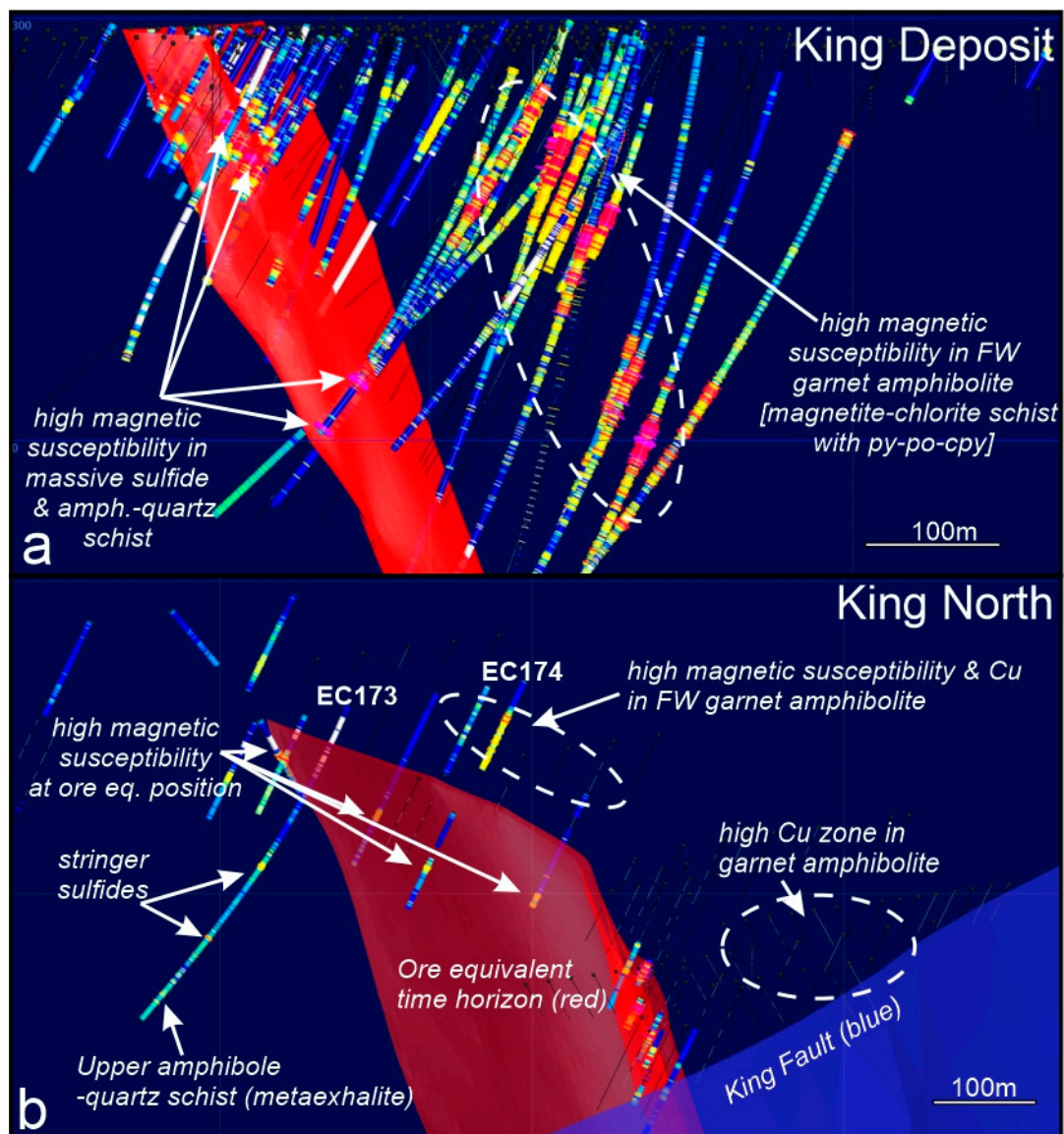


Figure 14. Leapfrog model showing magnetic susceptibility measurements (colors: dark blue to hot pink increasing scale) from the King deposit (a), and at King North (b). The modeled massive sulfide lens is shown in red for the King deposit, and the equivalent stratigraphic horizon at King North. The King Fault is shown in blue. Note the high magnetic susceptibility measurements associated with the amphibole–quartz schist at King (in the immediate hanging-wall) and within the garnet amphibolite associated with abundant chlorite–magnetite in the deep footwall.

Compared to all other rocks described, the FIII rhyolites at King North are relatively enriched in Al_2O_3 and K_2O (typically >10 wt%; and 1–4 wt%, respectively). Fe_2O_3 contents (2–23 wt%) exhibit a similar range to the FII-affinity chlorite–quartz schists. Sulfur contents are fairly low but approach 7 wt% in some samples. On the box plot of Large et al. [48], data trend between the least altered box towards the pyrite–chlorite node, on a pyrite–chlorite (–sericite) trend. Most trace metals of interest for VMS exploration are strongly correlated in these rocks. Copper, for example, is extremely strongly correlated with Au–Ag (>0.9), and slightly less so with Bi–Mo–Sn–Te–W (0.7–0.8) and Zn–Sb–Tl (0.5–0.7). Lead and Ni are poorly to weakly correlated with all other elements, except Sb in the case of Ni.

Chlorite–actinolite–quartz schist (meta-exhalite): the chlorite–actinolite–quartz schist is characterized by very high Fe_2O_3 (>25 wt%) and variable S (3 to $>10\%$), MgO (0.9–8.4 wt%), Al_2O_3 (2.8–12.5 w%), and CaO (0.9–7.7 wt%) contents. Na_2O and K_2O contents are low

(<1.8 wt% and <0.6 wt%, respectively). Base metal and precious metal contents are anomalous to high: 375–12,500 ppm Cu, 232–1820 ppm Zn, 1–14 ppm Ag, 0.1–3.2 g/t Au.

Amphibole–quartz–albite schists (andesitic): these rocks are characterized well through litho-geochemistry, petrography, and XRD analysis. They are of intermediate composition, plotting within the andesite field of the Winchester and Floyd [49] diagram (the ‘HW metasedimentary rocks’ of Figures 10d and 12e). These rocks straddle the calc-alkaline and high-K fields of Hastie et al. [51] due to high Th content (0.6 to 24.2 ppm; Figure 10a). Co and Cr contents are extremely variable (2–685 ppm and 3–430 ppm, respectively). LREE profiles (La/Sm_{CN} 2.1–3.2) and HREE profiles are gently to moderately dipping (Gd/Yb_{CN} 1.2–3.8) (Figure 12e). The quartz–epidote–chlorite–albite schists are of similar compositions and have identical REE profiles to the argillaceous metasedimentary rocks in the immediate hanging-wall of the King deposit. This includes both garnet-rich and strongly banded metasedimentary rocks (Figure 12e).

On the box plot of Large et al. [48], these rocks plot largely within the least altered andesite/basalt field but show considerable scatter toward the dolomite–ankerite, chlorite–pyrite, and sericite mineral nodes (not shown). Major element data also show considerable scatter—particularly Fe₂O₃ (1.0–50.3 wt%), MgO (0.1–15.5 wt%), CaO (<0.1–21.0 wt%), S (<0.1 to 10 wt%), and SiO₂ (53.0–66.2 wt%). No trends are apparent between major element pairs, except K–Al and Fe–S. These observations are consistent with a mixed sedimentary–volcaniclastic protolith. Several trace metal pairings are clear in the data, with relatively strong correlations (0.5–0.75) between Zn–Cu–Au–Ag–Cd±Pb and between Cu–Bi–Mo–Sn–Te–W.

Hanging-wall amphibolites (basaltic–andesitic): the hanging-wall amphibolites at King North are all of mafic to intermediate composition, plotting predominantly in the sub-alkaline basaltic andesite field of Winchester and Floyd [49] (Figure 10d). Their high Th concentrations and immobile element ratios suggest that the rocks are of transitional to calc-alkaline affinity (Figure 11a). These rocks are indistinguishable from the hanging-wall amphibolites at King in terms of their immobile element geochemistry [8]. They are characterized by flattish REE profiles (Figure 12d), with slight LREE enrichment in some samples (La/Sm_{CN} 1.0–2.1) and HREE enrichment in others (Gd/Yb_{CN} 1.2–2.1).

On the box plot, the hanging-wall amphibolites occupy a field between unaltered basalt and the Fe–Mg carbonate mineral nodes, with a subtle trend towards the chlorite–pyrite mineral node (Figure 11c). Interestingly, they appear slightly more altered (higher CCPI) than their correlatives at King. The mobile element geochemical characteristics of the amphibolites are characterized by moderate Fe₂O₃ (10.2–15.6 wt%), high CaO (7.2–17.1 wt%), variable MgO (3.3–11.9 wt%), and low SiO₂ (47.9–54.2 wt%) typical of quartz–epidote-altered mafic rocks. Most trace metals of interest (except Ni) are strongly correlated (>0.5): Au–Ag–Zn–Pb–Cu–Bi–Cd–Mo–Sb–Sn–Te–Tl–W, particularly Bi–Te (0.91), Cd–Zn (0.8), and Cu–Au (0.77).

Muscovite–chlorite schist (andesitic to dacitic): narrow units of soft muscovite–chlorite schist were intercepted in the King North diamond hole EC173D at depths between 235 and 260 m (Figures 7 and 8e). These rocks are characterized by high MgO (20.4–22.0 wt%), variable Fe₂O₃ (4.9–13.1), CaO (0.8–5.9 wt%), and Al₂O₃ (8.1–13.2 wt%), plus low TiO₂ (0.5–0.8 wt%), Cr (100–1480 ppm), and SiO₂ (45.6–51.8 wt%). Their high Zr/TiO₂ ratios are indicative of a dacitic protolith.

Hanging-wall muscovite–quartz schists (dacitic to rhyolitic): leucocratic quartz–sericite-altered schists intercepted in EC173D are of felsic composition and range from FII-affinity dacites (samples KN12,13) to FIII-affinity rhyolites (samples KN09,10) (Figures 10e and 12f). These rocks are geochemically identical to the lithologies already described from the shallower RC drilling (see Figure 10c). These rocks plot within the least altered dacite and rhyolite fields of the alteration box plot and have notably lower CCPI than the footwall felsic schists from RC drilling (Figure 11d). Sulfur contents are variable but low (0.02–1.37 wt%). Base metal contents are low (maximum values: 104 ppm Zn, 33 ppm Cu, 22 ppm Pb).

Amphibole–quartz schist (upper exhalite): a thin unit of amphibole–quartz schist intercepted at depth in hole EC173D (Figure 7; 340 m) is dominated by high SiO₂ (69.2 wt%) and Fe₂O₃ (23.2 wt%), with low CaO (2.8 wt%), MgO (2.4 wt%), and S (0.2 wt%). This rock displays a gently dipping chondrite-normalized REE profile, similar to the amphibole–quartz schist in the hanging-wall to the massive sulfide mineralization at King, but displays a prominent negative Eu anomaly (instead of a positive Eu anomaly). Base metal contents are low (e.g., 98 ppm Zn, 5 ppm Cu).

7. Discussion

7.1. Geology of the King North Prospect and Correlations with the King Area

From the extensive petrographic, litho-geochemistry, and XRD results presented here, it is evident that the volcanic–sedimentary package of rocks drilled at King North are similar in their mineralogy and geochemical evolution to those previously described from 2.5 km further south at King [8], albeit with several significant differences. Both sequences are overturned, dipping to the east, and are now separated by the NE–SW trending King Fault (Figures 4 and 13a). The entire volcanic sequence was deposited in a deep-marine, rifted-arc or cratonic rift, setting at c. 2.70 Ga. A comparison between the stratigraphic successions of both areas is presented in Figure 15.

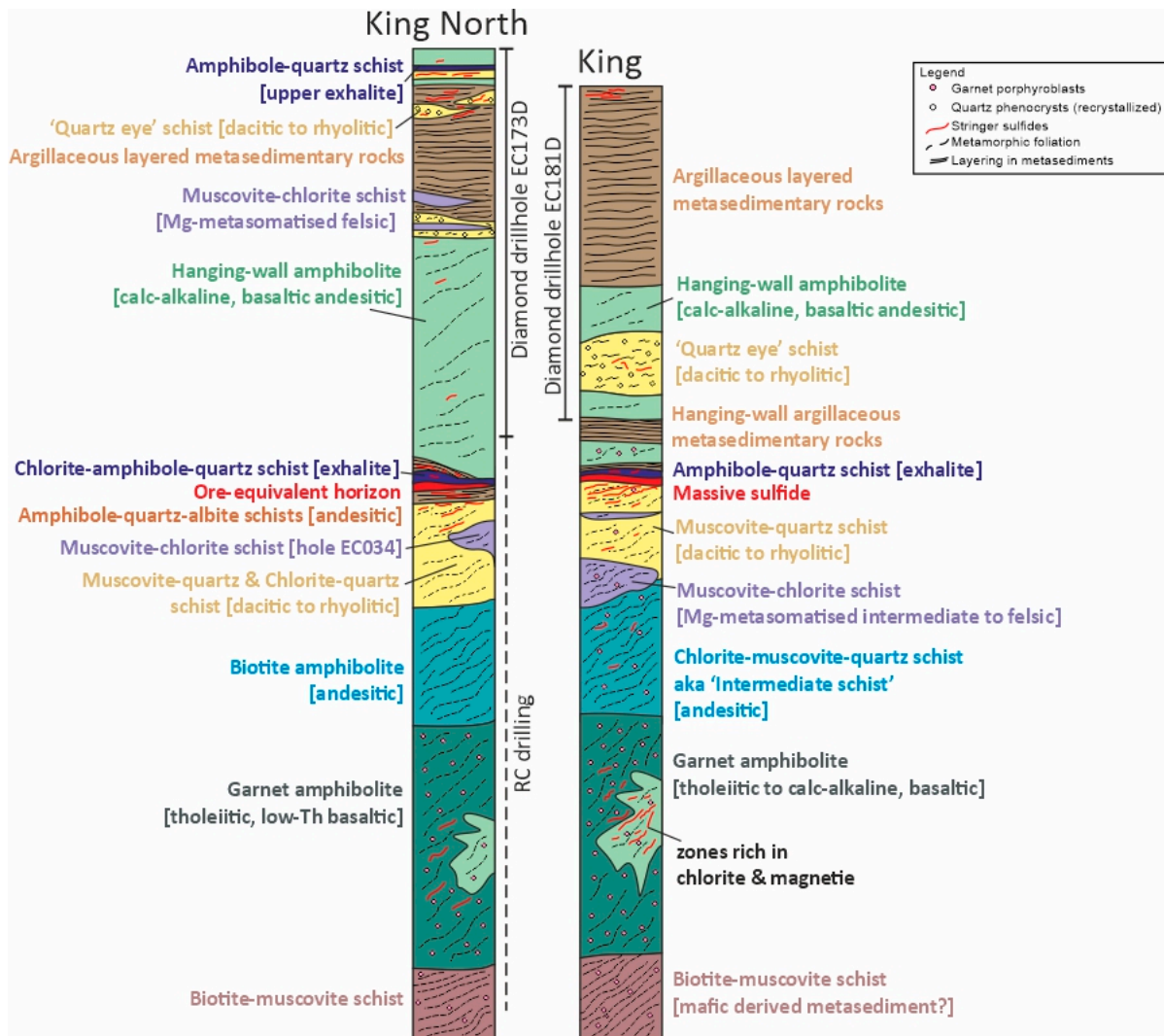


Figure 15. Comparison between the greenstone belt stratigraphy at King North and through the King deposit.

Deep mafic footwall: the deepest rocks of the greenstone belt are the mineralogically complex and strongly banded, *biotite–muscovite schists*. Although these rocks were not identified in rock chips on the central section line at King North (Figure 5), they were logged to underlie garnet amphibolite to the east by company personnel. Rock chips of biotite–muscovite schist have been identified from holes collared NE of EC174 by Black Raven Mining (Figure 12c), close to the King Fault (Figure 13a). Immobile element geochemical characteristics of the biotite–muscovite schists are consistent with protoliths of broadly mafic composition (Figure 10a). When coupled with their very high Al_2O_3 (13.8–21.5 wt%) and elevated K_2O (predominantly 3.3–4.9 wt%) contents, banded nature, and highly variable mineralogy, this suggests that they represent mafic-derived metasedimentary rocks with a fluctuating felsic component. With depth, the biotite–muscovite schists often show systematic variations in the abundance of biotite, white mica, chlorite, and quartz. In several diamond drillholes they also occur interbedded within the overlying garnet amphibolite (interpreted meta-basalts) at the meter to decimeter scale (Supplementary Figure S2). In the deep footwall of the King deposit, the biotite–muscovite schists are characterized by high alteration index and Carbonate–Chlorite–Pyrite Index values (Figure 11c) and anomalous metal contents (Cu–Zn–Ag–Au–Cd–Bi–Te), which suggests that they were mineralized and hydrothermally altered prior to metamorphism.

At King North, the next highest unit identified in RC drilling through petrography and lithochemistry is a sequence of *garnet amphibolite* at least 100 m thick (Figures 5 and 12c). Low Ti/V ratios and Th contents from the garnet amphibolites suggest that the protolith was likely a low-Ti tholeiitic basalt. Mineralogically identical rocks occur along strike at King, at a similar position in the greenstone belt (Figure 12a), though these are characterized by notably higher Ti/V ratios (Figure 10f). No primary volcanic textures are preserved at either locality.

Within the package of garnet amphibolites at King there is also a broad zone characterized by abundant chlorite and disseminated magnetite and ilmenite. This is reflected in high magnetic susceptibility measurements associated with these rocks throughout the deep footwall (Figure 14a). It was proposed by Hollis et al. [8] that this represents a zone of intense Mg–Fe alteration in the feeder zone of the overturned King deposit prior to metamorphism. These chloritic mafic rocks are coincident with abundant stringer and disseminated Fe–Cu sulfides—typically pyrite, pyrrhotite and chalcopyrite—recrystallized into the regional foliation. By contrast, Mg-metasomatized intermediate to felsic rocks in the feeder zone (discussed below) are represented by a thick package of *muscovite–chlorite schist* (Figure 13a). Similar zones rich in chlorite and magnetite likely exist within the broader garnet amphibolite unit in drill hole EC174 at King North (Figure 5), and 1 km further south towards the King Fault near hole EC034 (Figure 4). Garnet amphibolite in these areas has notably higher Cu contents and magnetic susceptibility values (Figure 14b).

Intermediate to felsic footwall: the garnet amphibolite sequence at King North is overlain by a sequence of *biotite amphibolite* of intermediate composition. These rocks are geochemically equivalent to the mineralogically complex ‘mixed footwall sequence’ of intermediate schists at King described by Hollis et al. [8]. At King, equivalent rocks often occur as chlorite–muscovite–quartz schists or are strongly banded, with individual layers dominated by either amphibole, epidote, quartz, chlorite, white mica, carbonate, or biotite (Figure 15). At King North, these intermediate schists appear to be interbedded with garnet amphibolite in holes EC163 and EC174 (Figure 5). The varying mineralogy of the intermediate schists across the greenstone belt likely represents different styles and intensities of hydrothermal alteration prior to regional metamorphism.

Stratigraphically above the mixed intermediate package of rocks at King North is a more felsic package of mixed *chlorite–quartz schist* and *muscovite–quartz schist* at least 90 m thick (Figure 15). These include both dacitic rocks of FI to FII affinity, and more rhyolitic rocks of FII to FIII affinity (Figures 10c and 11b). As stated earlier, the King Zn deposit occurs at the stratigraphic top of an equivalent felsic-dominated package (Figures 13a and 15), with its stringer zone extending into the lower intermediate to mafic stratigraphy [8].

Together, these felsic rocks represent the culmination of a volcanic cycle and the progressive evolution of the volcanic sequence from tholeiitic and calc-alkaline mafic lavas, through andesitic and dacitic, to HFSE-enriched rhyolitic compositions. Due to the strong degree of deformation and metamorphism, the exact volcanological relationship between the dacitic and rhyolitic rocks is not clear. Given the thickness of the latter (Figure 5), and the viscosity of rhyolitic lavas, these rocks may either represent thin coeval sills intruded into the evolving volcanic pile or accumulations of volcanoclastic rocks.

Hanging-wall sequence: following the deposition of the felsic volcanic/volcanoclastic rocks at King North, a sequence of metasedimentary rocks of intermediate composition were deposited (the *amphibole–quartz–albite schists*). This package represents a prolonged hiatus in volcanic activity and appears to thicken rapidly across the central line of drilling towards the east (from <5 to ~30 m thick), particularly between holes EC175 and EC173 (Figure 5). This is indicative of a syn-volcanic fault in the vicinity, which is discussed below in relation to VMS mineralization. Similar metasedimentary rocks occur stratigraphically above the King deposit [8]. The *chlorite–actinolite–quartz schist* of hole EC175 at King North is interpreted as a meta-exhalite, equivalent to the *amphibole–quartz schist* along strike that directly overlies the King deposit (Figure 15). Actinolite and chlorite are retrograde alteration productions of grunerite and hornblende at King. This unit at King North is also associated with high magnetic susceptibility measurements, as at King (Figure 14a).

Lithologies overlying these metasedimentary rocks include a: (i) ~130 m thick package of amphibolites of calc-alkaline basaltic andesite affinity (the *hanging-wall amphibolites*), (ii) a ~100 m thick mixed sequence of interbedded argillaceous metasedimentary rocks and felsic volcanoclastic rocks, (iii) an upper amphibole–quartz schist (an upper, second meta-exhalite at King North), and (iv) further package of amphibolite/meta-basalt (Figure 15). Equivalent units have been intercepted by recent diamond drilling into the deep stratigraphic hanging-wall of the King deposit (i.e., hole EC181D) as shown in Supplementary Figure S3.

7.2. An Overtuned VMS System at King North

Mobile element trends and metal correlations are consistent with King North representing part of an overturned VMS system, with the principal feeder zone and overlying ore lens awaiting discovery. Evidence includes its observed mineralogy, significant metal/metalloid enrichments, high alteration index values, and several intercepts of Zn-Cu-Au mineralization.

Hydrothermal alteration around VMS systems is well understood and described in the literature [40,53,54]. In volcanic rocks that have experienced greenschist facies metamorphism, several distinct styles of hydrothermal alteration can occur, dominated by the abundance of the following minerals: quartz, chlorite, white mica (muscovite, paragonite, phengite), carbonate, and albite [48]. The principal feeder zone is typically characterized by abundant chlorite and Fe-Cu sulfides due to intense Fe-Mg metasomatism [40,53]. Surrounding rocks are often dominated by quartz, sericite, and lesser chlorite, particularly those of felsic composition. By contrast, at amphibolite to granulite metamorphic grade, these relatively simple alteration patterns are obscured by complex mineralogical assemblages that often also include the following: garnet, amphibole, biotite/phlogopite, staurolite, cordierite, kyanite/sillimanite/andalusite, chloritoid, and/or gahnite [40,55]. Metamorphism at both King and King North is mid-amphibolite grade in the east (proximal to the late granitoid intrusions) and decreases to upper greenschist facies in the stratigraphic hanging-wall [8].

Along strike at King, felsic footwall schists are dominated by quartz, muscovite, and chlorite, and mafic lithologies by garnet, amphibole, quartz, chlorite, magnetite, and ilmenite [8]. Epidote is common in mafic lithologies around granitic intrusions. This is similar to the observed mineralogy in shallow RC drilling at King North, where quartz, muscovite, and chlorite dominate the mineralogy of felsic rocks, and chlorite and magnetite are increasingly common in mineralized intervals of garnet amphibolite. All footwall lithologies yield high AI and CCPI values, with analyses trending towards the carbonate and pyrite–chlorite (–magnetite) mineral nodes (Figure 11c,d). Some scatter also exists

towards the sericite node in felsic lithologies. High to anomalous concentrations of Bi-Cd-Sb-Sn-Te-Tl-W in footwall rocks are similar to myriad VMS deposits globally [3,37,40,54].

As expected for VMS systems, the hanging-wall lithologies at King North are significantly less altered than the footwall rocks (Figure 11c,d) and characterized by higher contents of carbonate and albite [48,53,56]. Normative corundum values are also a useful tool for distinguishing least-altered hanging-wall rocks from hydrothermally altered footwall strata in metamorphosed VMS deposits [8,37]. Alkali leaching in the footwall of a VMS deposit will result in excess Al over Ca+Na+K, and therefore high calculated CIPW normative corundum values [37]. By contrast, least-altered or unaltered hanging-wall strata will yield values ~0%. At King North, normative corundum values are typically between 5–20 wt% in footwall felsic rocks, ~6–7% around zones of base metal mineralization in hole EC175, and 0 wt% stratigraphically above mineralization (holes EC175 and EC164; Figure 5).

7.3. Implications for Exploration at King North

Considering their stratigraphic similarities, the massive sulfide equivalent horizon from the King deposit can now be traced along strike to King North (Figure 13a). At the latter, this occurs around the top of the felsic schists (the *chlorite-quartz schists* and *muscovite-quartz schists*), with minor mineralization also towards the base of the overlying metasedimentary package (the *amphibole-quartz-albite schists*) (Figure 5). Mineralization is typically Fe- (Zn-) dominated (e.g., 20 m at 0.1% Zn), with significant gold associated with the Fe-rich *chlorite-actinolite-quartz schist* (11 m at 0.52 g/t Au) near a hypothesized syn-volcanic fault. The latter occurs broadly parallel to drill hole EC179 (Figure 5). Copper mineralization occurs both around hole EC179 and deeper in the volcanic pile within the garnet amphibolite (Figure 5). Significant room exists at King North for the discovery of lenses of massive sulfides: (i) to the north, associated with an untested Zn soil anomaly, (ii) down-dip of current shallow AC, RAB, and RC drilling in the central region, and (iii) further south, associated with intensely Mg-metasomatized felsic rocks near hole EC034 (discussed below; Figure 4). All existing drilling is to shallow levels (<100 m vertical depth), with the exception of hole EC173D.

In the King footwall sequence, a thick package of soft *muscovite-chlorite schist* has been identified (Figure 13a; Supplementary Figure S1). This represents a key alteration lithology for regional exploration across the entire greenstone belt. This unit is ~80 m thick under the center of the King deposit within the intermediate to felsic schists, and thins rapidly along strike (Figure 13a,b). These rocks are characterized by very high MgO (9.6–32.9 wt%) and low SiO₂ (31.4–50.8 wt%) contents. Whilst these compositions are reminiscent of ultramafic or primitive mafic magmas (komatiites and/or high Mg basalts), this is not consistent with their very low Cr (<216 ppm), Ni (<71 ppm), and Co (<18 ppm) contents and high Al₂O₃ values (11.8–25.5 wt%). For comparison, spinifex-textured komatiite flows associated with the c. 2705 Ma Nimbus deposit contain 2230–2880 ppm Cr, 742–1480 ppm Ni, 83–95 ppm Co, and 4.4–7.1 wt% Al₂O₃ [20]. The muscovite-chlorite schists at King also contain abundant zircon and have intermediate to felsic compositions when plotted on both the Winchester and Floyd [49] and Hastie et al. [51] discrimination diagrams. These rocks were most likely formed due to intense Mg-metasomatism and alkali leaching in the intermediate to felsic footwall rocks of the King VMS deposit. Very high AI and CCPI values place these rocks entirely in the 'ore corner' of the box plot (Figure 11d). In the central region of drilling at King North (Figure 5), several units of muscovite-chlorite schist <5 m thick been identified in the deep diamond tail of hole EC173D (20–22 wt% MgO) associated with FIII-affinity felsic rocks in the hanging-wall stratigraphy (Figure 7; 240 m). However, further south in RC hole EC034 (Figure 4a), a zone of Mg-metasomatism (~15 wt% MgO) occurs within the felsic package just below the ore-equivalent horizon across five holes and ~200 m of strike. This area is also coincident with a significant Zn soil anomaly (Figure 4b). The muscovite-chlorite schist is thickest (~10 m) in hole EC034 and thins to the north, but is

untested to the south and east of EC034. Characterizing the extent and orientation of this zone of Mg-metasomatism represents a key objective for further exploration at King North.

The recognition of abundant HFSE-enriched rhyolites at King North is also significant. Leshner et al. [52] helped to distinguish VMS-prospective and barren felsic rocks, defining three geochemically distinct groups of felsic volcanic rocks - FI, FII, and FIII rhyolites. This was later refined by Hart et al. [57] to include FIV rhyolites associated with post-Archaeon terranes. All VMS occurrences in the Yilgarn Craton are associated with HFSE-enriched, FIII-affinity felsic rocks [2], apart from the Nimbus deposit that formed in shallower waters over thickened crust away from the main Teutonic rift zone [20,56]. Significantly, these FIII-affinity, HFSE-enriched rhyolitic rocks are common at King North near the massive sulfide equivalent horizon (Figure 5), and also occur higher in the volcanic stratigraphy (e.g., Figure 7, 230 m depth). This observation suggests formation within an Archaean rift sequence from high temperature (>900 °C) melts, derived from melting of hydrated basaltic crust at shallow depths during extension [58,59].

7.4. Stacked VMS Potential in the King Greenstone Belt?

Recent diamond drilling into the hanging-wall sequence of VMS mineralization at King and King North (Figures 7 and 15) has refined our understanding of the regional stratigraphy. It is now clear that there are a number of volcanic cycles, showing a broad geochemical evolution from rocks of basaltic affinity, through andesitic compositions, to dacites and HFSE-enriched rhyolites. This geochemical evolution is evident in greenstone belts of both the Edjudina and Murrin domains (Figure 2) though, in the latter, magmas rarely reached rhyolitic compositions [14]. VMS mineralization typically occurs towards the end of each eruptive cycle, during a hiatus in volcanic activity, and is locally accompanied by evidence of seafloor exhalation during background deep-marine sedimentation. Volcanic cyclicity is well recognized from VMS camps worldwide [40], with the switch back to mafic volcanism often due to further extension and the tapping of mantle-derived melts. Although multiple VMS prospective stratigraphic horizons can be present within individual camps, typically one of these will contain the majority of the metal endowment [60].

At King North, the chlorite–actinolite–quartz schist (meta-exhalite), at the massive sulfide equivalent horizon, and the amphibole–quartz–albite schists (overlying meta-sedimentary rocks) represent the culmination of cycle one (Figure 5). This is the along-strike equivalent of the King K1 stratigraphy of Figure 3, represented by garnet amphibolite (meta-basalt), intermediate to felsic schists, and capped by amphibole–quartz schist (meta-exhalite) and fine-grained metasedimentary rocks of the immediate hanging-wall (Figure 15).

A second VMS-prospective horizon in the younger hanging-wall sequence is indicated by the presence of the amphibole–quartz schist in hole EC173D (Figure 8h), associated with hydrothermally altered felsic schists (of FII to FIII affinity), pyrrhotite–pyrite-rich fine-grained sedimentary rocks (Figure 8g), and minor occurrences of muscovite–chlorite schist (Figure 7). Any EM conductors associated with this stratigraphic package along strike can now be considered targets for VMS mineralization. It is important to note that this upper amphibole–quartz schist at King North lacks a positive Eu anomaly, which is typical of VMS-proximal exhalites globally [61–65] and is associated with low magnetic susceptibility measurements and base metal values (Cu+Zn 103 ppm). It is considered to represent an exhalite more distal to massive sulfide mineralization. Due to the reduced metamorphic grade in the hanging wall stratigraphy (to the west), the original volcanic architecture will be easier to delineate, along with any syn-volcanic faults that may have focused hydrothermal fluids.

Little is known about the overlying K2 package of the Edjudina Domain (see Figure 3), due to poor outcrop and very limited drilling. It was re-mapped based on regional airborne magnetics and divided into the Colby BIF and Colby Schists (Figure 3). The latter is a mixed sequence of meta-basalt, metasedimentary rocks, and undifferentiated schist. The Colby BIF is significantly thicker (10 to >50 m) and more laterally extensive than the

amphibole–quartz schist at King. The unit is readily identifiable in airborne magnetics and can be used as a stratigraphic marker. Regionally, it is often thickened due to folding and fault repetition. It is interpreted to represent more stable deep marine conditions and the deposition of ambient chemical pelagite, and is not believed to be related to the exhalation of hydrothermal fluids.

An additional VMS-bearing package of volcanic rocks occurs immediately west of the Claypan Fault [14], the K3 sequence of Figure 3, located in the Murrin Domain. This sequence was defined by several diamond drillholes across ~3.2 km along strike of stratigraphy and has been described in detail by Hollis et al. [14]. U-Pb zircon geochronology constrains its age to c. 2685–2680 Ma (Figure 2). Significant intercepts of Zn mineralization (e.g., EC155D: 19 m at 0.4% Zn) occur in a 50–75 m thick, mixed package of felsic volcanic/volcaniclastic and argillaceous rocks. The latter includes thick sequences of black shale. Massive pyrite was intercepted (1.4–1.7 m thick) in two southern diamond drillholes 300 m apart (holes EC157D and EC158D; Figure 3). The VMS-prospective package is underlain by ~100 m of intermediate volcanoclastic rocks and a sequence of meta-basalt at least 150 m thick in the northernmost drillhole EC156D (Figure 3). The hanging-wall sequence is marked again by the return of mafic volcanism and is at least 150 m thick. Several additional target areas have also been identified along strike, associated with EM and soil geochemical anomalies [14].

8. Conclusions

Through extensive core logging, petrography, SEM imaging, XRD analysis, and litho-geochemistry, the King North stratigraphy has been characterized and correlations made with the King area.

The overturned footwall stratigraphy at King North is dominated by variably metamorphosed and hydrothermally altered volcanic rocks, namely the following: garnet amphibolite (tholeiitic, basaltic), biotite amphibolite (andesitic, calc-alkaline), and chlorite–quartz schist (dacitic), with narrow horizons of muscovite–quartz schist (rhyolitic, HFSE-enriched). The hanging-wall to the Zn-bearing sequence is characterized by quartz–albite schists (metasedimentary rocks) and thick sequences of amphibolite (calc-alkaline, basaltic andesite). An iron-rich unit (>25% Fe₂O₃) of chlorite–actinolite–quartz schist, interpreted as a meta-exhalite, is associated with significant Cu–Au mineralization, adjacent to a possible syn-volcanic fault. The overlying stratigraphy includes thick sequences of amphibolite (meta-basalt) and interbedded felsic volcanic/volcaniclastic and argillaceous metasedimentary rocks.

Hydrothermal alteration assemblages and geochemical characteristics at King North (Mg–Si–K-enrichment, Na-depletion, and high Sb, Tl, Eu/Eu*, alteration index, CCPI, normative corundum abundance values) are consistent with a second overturned VMS system. Extensive Mg-metasomatism of the felsic footwall (now muscovite–chlorite schists) occurs in the southern area of drilling.

Recent diamond drilling into the hanging-wall at King and King North indicates the stacked VMS potential of the regional stratigraphy east of the Claypan Fault. This includes the discovery of HFSE-enriched (FIII-affinity) rhyolites, zones of intense Mg-metasomatism, presence of abundant sulfide-rich argillaceous metasedimentary rocks, and a second meta-exhalite.

Through our approach, we demonstrate that, through detailed logging of rock chips, petrography, and litho-geochemistry, complex volcanic stratigraphies can be established across variably metamorphosed greenstone belts, and VMS alteration signatures recognized. This has wider implications for more cost-effective exploration across the Yilgarn Craton, with RC drilling used primarily to reconstruct the local geology and identify proximal halos. More costly diamond drilling is limited to key areas of complex geology and deeper EM targets.

Supplementary Materials: The following supporting information can be downloaded at: <https://www.mdpi.com/article/10.3390/min14050481/s1>, Figure S1: Base metal classification scheme for VMS deposits after [38–40], with the fields for Cyprus-, Abitibi-, and Kuroko-type deposits of the Urals from [41]. Samples of massive sulfide from King are shown along with significant intercepts of mineralization at King North; Figure S2: Summary geological log of diamond drillhole EC153D through the King footwall stratigraphy. See Figure 10d for the location of this hole; Figure S3: Summary geological log of diamond drillhole EC181D through the King hanging-wall stratigraphy. Much of the stratigraphic footwall has been removed by the King Fault or an adjacent splay. See Figure 10d for the location of this hole; Table S1: Whole-rock geochemical data from King North and King; Table S2: XRD results of rock chips analyzed from RC drillholes.

Author Contributions: Conceptualization, J.K., S.P.H., D.P., M.J. and S.R.; Formal analysis, J.K., S.P.H., C.D.P.D., A.K., M.J., R.A. and C.R.; Funding acquisition, D.P.; Investigation, J.K., S.P.H., C.D.P.D., A.K., M.J., R.A. and C.R.; Methodology, J.K., S.P.H. and C.D.P.D.; Project administration, D.P. and S.P.H.; Software, A.K. and S.P.H.; Supervision, S.P.H., D.P. and S.R.; Visualization, A.K., M.J. and R.A.; Writing—original draft, J.K. and S.P.H.; Writing—review and editing, J.K., S.P.H., C.D.P.D., A.K., D.P., M.J., R.A., C.R. and S.R. All authors have read and agreed to the published version of the manuscript.

Funding: Black Raven Mining are thanked for funding whole-rock geochemistry and for their support throughout the project. Cendi Dana acknowledges funding through a National Environment Research Council (NERC) Doctoral Training Partnership grant (NE/S007407/1). Diamond and RC drilling by Black Raven Mining was co-funded through the Exploration Incentive Scheme of Western Australia.

Data Availability Statement: New data generated during this research are contained within the article and Supplementary Materials. Restrictions apply to the availability of the company litho-geochemical database.

Acknowledgments: This manuscript is based in part on the lead author’s undergraduate thesis at the University of Southampton, which focused on RC drilling at King North. The authors thank Ross Williams and Richard Pearce for supporting the XRD and SEM technical analysis at Southampton. Three anonymous reviewers are thanked for their constructive comments on this manuscript.

Conflicts of Interest: D.P., M.J., A.K. and R.A. are either employees of Black Raven Mining, or have undertaken contract work for Black Raven Mining. The paper reflects the views of the scientists and not the company.

References

1. Yeats, C.J. VHMS mineral systems in the Yilgarn—Characteristics and exploration potential. In Proceedings of the Geoconferences (WA) Inc. Kalgoorlie 07 Conference, Kalgoorlie, Australia, 25–27 September 2007; Bierlein, F.P., Ed.; Geoconferences Inc.: Perth, WA, USA, 2007; pp. 65–69.
2. Hollis, S.P.; Yeats, C.J.; Wyche, S.; Barnes, S.J.; Ivanic, T.J.; Belford, S.M.; Davidson, G.J.; Roache, A.J.; Wingate, M.T.D. A review of volcanic-hosted massive sulfide (VHMS) mineralization in the Archaean Yilgarn Craton, Western Australia: Tectonic, stratigraphic and geochemical associations. *Precambrian Res.* **2015**, *260*, 113–135. [[CrossRef](#)]
3. Hayman, P.C.; Hull, S.E.; Cas, R.A.; Summerhayes, E.; Amelin, Y.; Ivanic, T.J.; Price, D. A new period of volcanogenic massive sulfide formation in the Yilgarn: A volcanological study of the ca 2.76 Ga Hollandaire VMS deposit, Yilgarn craton, Western Australia. *Aust. J. Earth Sci.* **2015**, *62*, 189–210. [[CrossRef](#)]
4. Duuring, P.; Hassan, L.; Zelic, M.; Gessner, K. Geochemical and spectral footprint of metamorphosed and deformed VMS-style mineralization in the Quinns district, Yilgarn Craton, Western Australia. *Econ. Geol.* **2016**, *111*, 1411–1438. [[CrossRef](#)]
5. Barrote, V.R.; McNaughton, N.J.; Tessalina, S.G.; Evans, N.J.; Talavera, C.; Zi, J.-W.; McDonald, B.J. The 4D evolution of the Teutonic Bore Camp VHMS deposits, Yilgarn Craton, Western Australia. *Ore Geol. Rev.* **2020**, *120*, 103448. [[CrossRef](#)]
6. Van Kranendonk, M.J.; Ivanic, T.J.; Wingate, M.T.D.; Kirkland, C.L.; Wyche, S. Long-lived, autochthonous development of the Archaean Murchison Domain, and implications for Yilgarn Craton tectonics. *Precambrian Res.* **2013**, *229*, 49–92. [[CrossRef](#)]
7. Ivanic, T.J.; Wingate, M.T.D.; Kirkland, C.L.; Van Kranendonk, M.J.; Wyche, S. Age and significance of voluminous mafic-ultramafic magmatic events in the Murchison Domain, Yilgarn Craton. *Aust. J. Earth Sci.* **2010**, *57*, 597–614. [[CrossRef](#)]
8. Hollis, S.; Podmore, D.; James, M.; Menuge, J.F.; Doran, A.L.; Yeats, C.J.; Wyche, S. VHMS mineralisation at Erayinia in the Eastern Goldfields Superterrane: Geology and geochemistry of the metamorphosed King Zn deposit. *Aust. J. Earth Sci.* **2019**, *66*, 153–181. [[CrossRef](#)]
9. Huston, D.L.; Champion, D.C.; Cassidy, K.F. Tectonic controls on the endowment of Archaean cratons in VHMS deposits: Evidence from Pb and Nd isotopes. In *Mineral Deposit Research: Meeting the Global Challenge, Proceedings of the Eighth Biennial SGA Meeting, Beijing, China, 18–21 August 2005*; Mao, J., Bierlein, F.P., Eds.; Springer: Cham, Switzerland, 2005; pp. 15–18.

10. Huston, D.L.; Champion, D.C.; Cassidy, K.F. Tectonic controls on the endowment of Neoproterozoic cratons in volcanic-hosted massive sulfide deposits: Evidence from lead and neodymium isotopes. *Econ. Geol.* **2014**, *109*, 11–26. [[CrossRef](#)]
11. Sharpe, R.; Gemmill, J.B. Alteration characteristics of the Archean Golden Grove Formation at the Gossan Hill deposit, Western Australia: Induration as a focusing mechanism for mineralizing hydrothermal fluids. *Econ. Geol.* **2001**, *96*, 1239–1262. [[CrossRef](#)]
12. Belford, S.M.; Davidson, G.J.; McPhie, J.; Large, R.R. Architecture of the Neoproterozoic Jaguar VHMS deposit, Western Australia: Implications for prospectivity and presence of depositional breaks. *Precambrian Res.* **2015**, *260*, 136–160. [[CrossRef](#)]
13. Parker, P.; Belford, S.M.; Maier, R.; Lynn, S.; Stewart, W. Teutonic Bore-Jaguar-Bentley volcanogenic massive sulfide field. In *Australian Ore Deposits*; Phillips, G.N., Ed.; The Australian Institute of Mining and Metallurgy: Melbourne, Australia, 2017; pp. 167–172.
14. Hollis, S.P.; Podmore, D.; James, M.; Mole, D.R.; Turner, O.; Kneeshaw, A.; Beaton, R. Targeting VHMS mineralization at Erayinia in the Eastern Goldfields Superterrane using litho-geochemistry, soil chemistry and HyLogger data. *J. Geochem. Explor.* **2019**, *207*, 106379. [[CrossRef](#)]
15. Smith, R.E.; Perdrix, R.L. Pisolithic laterite geochemistry in the Golden Grove massive sulfide district, Western Australia. *J. Geochem. Explor.* **1983**, *18*, 131–164. [[CrossRef](#)]
16. Smith, R.E.; Singh, B. Recognizing, in lateritic cover, detritus shed from the Archean Gossan Hill Cu–Zn–Su volcanic-hosted massive sulphide deposit, Western Australia. *Geochem. Explor. Environ. Anal.* **2007**, *7*, 71–86. [[CrossRef](#)]
17. Gray, D.J.; Yeats, C.J.; Noble, R.R.P.; Reid, N. Hydrogeochemical exploration for volcanic-hosted massive sulfide deposits in semi-arid Australia. *Aust. J. Earth Sci.* **2018**, *65*, 249–274. [[CrossRef](#)]
18. Yeats, C.J.; Groves, D.I. The Archean Mount Gibson gold deposits, Yilgarn Craton, Western Australia: Products of combined synvolcanic and syntectonic alteration and mineralisation. *Ore Geol. Rev.* **1998**, *13*, 103–129. [[CrossRef](#)]
19. Hassan, L.Y. *The Yuinmery Volcanogenic Massive Sulfide Prospects: Mineralization, Metasomatism and Geology*; Geological Survey of Western Australia: Perth, WA, Australia, 2014; Report 131; Volume 65.
20. Hollis, S.P.; Mole, D.R.; Gillespie, P.; Barnes, S.J.; Tessalina, S.; Cas, R.A.F.; Hildrew, C.; Pumphrey, A.; Goodz, M.D.; Caruso, S.; et al. 2.7 Ga plume associated VHMS mineralization in the Eastern Goldfields Superterrane, Yilgarn Craton: Insights from the low temperature and shallow water, Ag–Zn–(Au) Nimbus deposit. *Precambrian Res.* **2017**, *291*, 119–142. [[CrossRef](#)]
21. Champion, D.C.; Cassidy, K.F. An overview of the Yilgarn Craton and its crustal evolution. *Geosci. Aust. Rec.* **2007**, *14*, 8–13.
22. Mole, D.R.; Fiorentini, M.L.; Cassidy, K.F.; Kirkland, C.L.; Thebaud, N.; McCuaig, T.C.; Doublier, M.P.; Duuring, P.; Romano, S.S.; Maas, R.; et al. Crustal evolution, intra-cratonic architecture and the metallogeny of an Archean craton. *Geol. Soc. Lond. Spec. Publ.* **2013**, *393*, SP393–8. [[CrossRef](#)]
23. Cassidy, K.F.; Champion, D.C.; Krapež, B.; Barley, M.E.; Brown, S.J.A.; Blewett, R.S.; Groenewald, P.B.; Tyler, I.M. *A Revised Geological Framework for the Yilgarn Craton, Western Australia*; Western Australia Geological Survey: Perth, WA, Australia, 2006; Record 2006/8; 8p.
24. Pawley, M.J.; Wingate, M.T.D.; Kirkland, C.L.; Wyche, S.; Hall, C.E.; Romano, S.S.; Doublier, M.P. Adding pieces to the puzzle: Episodic crustal growth and a new terrane in the northeast Yilgarn Craton, Western Australia. *Aust. J. Earth Sci.* **2012**, *59*, 603–623. [[CrossRef](#)]
25. Barley, M.E.; Brown, S.J.A.; Krapež, B.; Kositcin, N. Physical volcanology and geochemistry of a Late Archean volcanic arc: Kurnalpi and Gindalbie Terranes, Eastern Goldfields Superterrane, Western Australia. *Precambrian Res.* **2008**, *161*, 53–76. [[CrossRef](#)]
26. Wyche, S.; Pawley, M.; Chen, S.; Ivanic, T.; Zibra, I.; Van Kranendonk, M.; Spaggiari, C.; Wingate, M. Geology of the northern Yilgarn Craton. In *Youanmi and Southern Carnarvon Seismic and Magnetotelluric (MT) Workshop*; Wyche, S., Ivanic, T.J., Zibra, I., Eds.; Geological Survey of Western Australia: East Perth, WA, Australia, 2013; Volume 6, pp. 33–65.
27. Jones, S.A. *Geology of the Erayinia 1: 100 000 Sheet*; Geological Survey of Western Australia: Perth, WA, Australia, 2007.
28. Wingate, M.T.D.; Bodorkos, S. 177919: Felsic metavolcanic rock, Urania Prospect; Geochronology dataset 666. In *Compilation of Geochronology Data*; Western Australia Geological Survey: Perth, WA, Australia, 2007.
29. Swager, C. *Geology of the Greenstone Terranes in the Kurnalpi-Edjudina Region, Southeastern Yilgarn Craton*; Geological Survey of Western Australia: Perth, WA, Australia, 1995; Volume 47.
30. Swager, C.P. Tectono-stratigraphy of late Archean greenstone terranes in the southern Eastern Goldfields, Western Australia. *Precambrian Res.* **1997**, *83*, 11–42. [[CrossRef](#)]
31. Nelson, D.R. 104973: Metadacite porphyry, east of Liberty Bore. In *Compilation of SHRIMP U–Pb Zircon Geochronology Data, 1994 (158–161)*; Western Australia Geological Survey: Perth, WA, USA, 1995; Record 1995/3.
32. Nelson, D.R. 104971: Metatonalite, Round Hill. In *Compilation of SHRIMP U–Pb Zircon Geochronology Data, 1995 (43–46)*; Western Australia Geological Survey: Perth, WA, USA, 1996; Record 1996/5.
33. Wingate, M.T.D.; Lu, Y.; Kirkland, C.L.; Spaggiari, C.V. 182419: *Granite Gneiss, Coonana Hill, Geochronology Record 1300*; Geological Survey of Western Australia: Perth, WA, Australia, 2016; 4p.
34. Fettes, D.; Desmons, J. Metamorphic rocks: A classification and glossary of terms. In *Recommendations of the International Union of Geological Sciences*; Cambridge University Press: Cambridge, UK, 2007.
35. Black Raven Mining. *Annual Report. For the Period 12 December 2017 to 11 December 2018*; Black Raven Mining: Canning Vale, Australia, 2019; 50p.
36. Black Raven Mining. *Annual Report. For the Period 19 December 2015 to 18 December 2016*; Black Raven Mining: Canning Vale, Australia, 2017; Erayinia Project C229/2007; 39p.

37. Grunsky, E.C. Predicting Archaean volcanogenic massive sulphide deposit potential from litho-geochemistry: Application to the Abitibi Greenstone Belt. *Geochem. Explor. Environ. Anal.* **2013**, *13*, 317–336. [[CrossRef](#)]
38. Franklin, J.M.; Lydon, J.W.; Sangster, D.F. Volcanic-associated massive sulfide deposits. In *Economic Geology 75th Anniversary Volume*; Skinner, B.J., Ed.; Society of Economic Geologists: Littleton, CO, USA, 1981; pp. 485–627.
39. Large, R.R. Australian volcanic-hosted massive sulphide deposits: Features, styles and genetic models. *Econ. Geol.* **1992**, *87*, 471–510. [[CrossRef](#)]
40. Galley, A.G.; Hannington, M.D.; Jonasson, I.R. Volcanogenic massive sulphide deposits. In *Mineral Deposits of Canada: A Synthesis of Major Deposit-Types, District Metallogeny, the Evolution of Geological Provinces, and Exploration Methods*; Geological Association of Canada, Mineral Deposits Division: St. John's, NL, Canada, 2007; Special Publication; Volume 5, pp. 141–161.
41. Lobanov, K.; Yakubchuk, A.; Creaser, R. A Besshi-type VMS deposits of the Rudny Altai (Central Asia). *Econ. Geol.* **2014**, *109*, 1403–1430. [[CrossRef](#)]
42. MacLean, W.H.; Barrett, T.J. Litho-geochemical techniques using immobile elements. *J. Geochem. Explor.* **1993**, *48*, 109–133. [[CrossRef](#)]
43. Jenner, G.A. Trace element geochemistry of igneous rocks: Geochemical nomenclature and analytical geochemistry. In *Trace Element Geochemistry of Volcanic Rocks: Applications for Massive Sulfide Exploration*; Wyman, D.A., Ed.; Geological Association of Canada: St. John's, NL, Canada, 1996; Short Course Notes; Volume 12, pp. 51–77.
44. MacLean, W.H. Mass change calculations in altered rock series. *Miner. Depos.* **1990**, *25*, 44–49. [[CrossRef](#)]
45. Boynton, W.V. Cosmochemistry of the rare earth elements: Meteorite studies. In *Developments in Geochemistry*; Elsevier: Amsterdam, The Netherlands, 1984; pp. 63–114.
46. Ishikawa, Y.; Sawaguchi, T.; Iwaya, S.; Horiuchi, M. Delineation of prospecting targets for Kuroko deposits based on modes of volcanism of underlying dacite and alteration halos. *Min. Geol.* **1976**, *26*, 105–117. (In Japanese with English Abstract)
47. Schardt, C.; Cooke, D.R.; Gemmell, J.B.; Large, R.R. Geochemical modeling of the zoned footwall alteration pipe, Hellyer volcanic-hosted massive sulfide deposit, Western Tasmania, Australia. *Econ. Geol.* **2001**, *96*, 1037–1054.
48. Large, R.R.; Gemmell, J.B.; Paulick, H. The Alteration Box Plot: A simple approach to understanding the relationship between alteration mineralogy and litho-geochemistry associated with volcanic-hosted massive sulfide deposits. *Econ. Geol.* **2001**, *96*, 957–971. [[CrossRef](#)]
49. Winchester, J.A.; Floyd, P.A. Geochemical discrimination of different magma series and their differentiation products using immobile elements. *Chem. Geol.* **1977**, *20*, 325–343. [[CrossRef](#)]
50. Shervais, J.W. Ti-V plots and the petrogenesis of modern and ophiolitic lavas. *Earth Planet. Sci. Lett.* **1982**, *59*, 101–118. [[CrossRef](#)]
51. Hastie, A.R.; Kerr, A.C.; Pearce, J.A.; Mitchell, S.F. Classification of altered volcanic island arc rocks using immobile trace elements: Development of the Th–Co discrimination diagram. *J. Petrol.* **2007**, *48*, 2341–2357. [[CrossRef](#)]
52. Leshner, C.M.; Goodwin, A.M.; Campbell, I.H.; Gorton, M.P. Trace-element geochemistry of ore-associated and barren, felsic metavolcanic rocks in the Superior Province, Canada. *Can. J. Earth Sci.* **1986**, *23*, 222–237. [[CrossRef](#)]
53. Piercey, S.J. The setting, style, and role of magmatism in the formation of volcanogenic massive sulfide deposits. *Miner. Depos.* **2011**, *46*, 449–471. [[CrossRef](#)]
54. Yeats, C.J.; Hollis, S.P.; Halfpenny, A.; Corona, J.-C.; LaFlamme, C.; Southam, G.; Fiorentini, M.; Herrington, R.J.; Spratt, J. Actively forming Kuroko-type volcanic-hosted massive sulfide (VHMS) mineralization at Iheya North, Okinawa Trough, Japan. *Ore Geol. Rev.* **2017**, *84*, 20–41. [[CrossRef](#)]
55. Dusel-Bacon, C. Petrology of metamorphic rocks associated with volcanogenic massive sulfide deposits. In *Volcanogenic Massive Sulfide Occurrence Model*; U.S. Geological Survey Scientific Investigations Report 2010-5070-C; U.S. Geological Survey: Reston, VA, USA, 2012; Chapter 17; 10p.
56. Hollis, S.P.; Foury, S.; Caruso, S.; Johnson, S.; Barrote, V.; Pumphrey, A. Litho-geochemical and hyperspectral halos to Ag–Zn–Au mineralization at Nimbus in the Eastern Goldfields Superterrane, Western Australia. *Minerals* **2021**, *11*, 254. [[CrossRef](#)]
57. Hart, T.R.; Gibson, H.L.; Leshner, C.M. Trace element geochemistry and petrogenesis of felsic volcanic rocks associated with volcanogenic massive Cu–Zn–Pb sulfide deposits. *Econ. Geol.* **2004**, *99*, 1003–1013. [[CrossRef](#)]
58. Barrie, C.T. Zircon thermometry of high-temperature rhyolites near volcanic-associated massive sulfide deposits. Abitibi subprovince, Canada. *Geology* **1995**, *23*, 169–172. [[CrossRef](#)]
59. Barrie, C.T.; Ludden, J.N.; Green, T.H. Geochemistry of volcanic rocks associated with Cu–Zn and Ni–Cu deposits in the Abitibi Subprovince. *Econ. Geol.* **1993**, *88*, 1341–1358. [[CrossRef](#)]
60. Gibson, H.; Galley, A. Volcanogenic massive sulphide deposits of the Archean, Noranda District, Quebec. In *Mineral Deposits of Canada: A Synthesis of Major Deposit-Types, District Metallogeny, the Evolution of Geological Provinces, and Exploration Methods*; Special Publication; Goodfellow, W.D., Ed.; Mineral Deposits Division, Geological Association of Canada: St. John's, NL, Canada, 2007; Volume 5, pp. 533–552.
61. Peter, J.M.; Goodfellow, W.D. Mineralogy, bulk and rare earth element geochemistry of massive sulphide-associated hydrothermal sediments of the Brunswick Horizon, Bathurst Mining Camp, New Brunswick. *Can. J. Earth Sci.* **1996**, *33*, 252–283. [[CrossRef](#)]
62. Peter, J.M.; Goodfellow, W.D. Hydrothermal sedimentary rocks of the Heath Steele Belt, Bathurst Mining Camp, New Brunswick. Part 3. Application of mineralogy and mineral and bulk compositions to massive sulfide exploration. *Econ. Geol. Monogr.* **2003**, *11*, 317–433.

63. Davidson, G.J.; Stolz, A.J.; Eggins, S.M. Geochemical anatomy of silica iron exhalites: Evidence for hydrothermal oxyanion cycling in response to vent fluid redox and thermal evolution (Mt. Windsor Subprovince, Australia). *Econ. Geol.* **2001**, *96*, 1201–1226. [[CrossRef](#)]
64. Binns, R.A. Data report: Petrography and geochemistry of jasperoids from site 1189, ocean drilling program Leg 193. In *Proceedings of the Ocean Drilling Program Scientific Results*; Barriga, F.J.A.S., Binns, R.A., Miller, D.J., Herzig, P.M., Eds.; Ocean Drilling Program: College Station, TX, USA, 2006; Volume 193, pp. 1–30. [[CrossRef](#)]
65. Hollis, S.P.; Cooper, M.R.; Herrington, R.J.; Roberts, S.; Earls, G.; Verbeeten, A.; Piercey, S.J.; Archibald, S.M. Distribution, mineralogy and geochemistry of silica-iron exhalites and related rocks from the Tyrone Igneous Complex: Implications for VMS mineralization in Northern Ireland. *J. Geochem. Explor.* **2015**, *159*, 148–168. [[CrossRef](#)]

Disclaimer/Publisher's Note: The statements, opinions and data contained in all publications are solely those of the individual author(s) and contributor(s) and not of MDPI and/or the editor(s). MDPI and/or the editor(s) disclaim responsibility for any injury to people or property resulting from any ideas, methods, instructions or products referred to in the content.